Journal of Hydrology 540 (2016) 397–411

Contents lists available at ScienceDirect

Journal of Hydrology

journal homepage: www.elsevier.com/locate/jhydrol

Conjunctive management of surface and groundwater resources under projected future climate change scenarios ☆

Amir Mani [a], Frank T.-C. Tsai [a,*], Shih-Chieh Kao [b,c], Bibi S. Naz [b,c], Moetasim Ashfaq [b,d], Deeksha Rastogi [b,d]

[a] Department of Civil and Environmental Engineering, Louisiana State University, 3526G Patrick F. Taylor Hall, Baton Rouge, LA 70803, USA
[b] Climate Change Science Institute, Oak Ridge National Laboratory, Oak Ridge, TN 37831, USA
[c] Environmental Sciences Division, Oak Ridge National Laboratory, Oak Ridge, TN 37831, USA
[d] Computer Science and Mathematics Division, Oak Ridge National Laboratory, Oak Ridge, TN 37831, USA

ARTICLE INFO

Article history:
Received 10 March 2016
Received in revised form 4 June 2016
Accepted 9 June 2016
Available online 16 June 2016
This manuscript was handled by Peter K. Kitanidis, Editor-in-Chief, with the assistance of Roseanna M. Neupauer, Associate Editor

Keywords:
Conjunctive use
Multi-reservoir system
Groundwater
Climate change
Uncertainty
Fractional programming

ABSTRACT

This study introduces a mixed integer linear fractional programming (MILFP) method to optimize conjunctive use of future surface water and groundwater resources under projected climate change scenarios. The conjunctive management model maximizes the ratio of groundwater usage to reservoir water usage. Future inflows to the reservoirs were estimated from the future runoffs projected through hydroclimate modeling considering the Variable Infiltration Capacity model, and 11 sets of downscaled Coupled Model Intercomparison Project phase 5 global climate model projections. Bayesian model averaging was adopted to quantify uncertainty in future runoff projections and reservoir inflow projections due to uncertain future climate projections. Optimized conjunctive management solutions were investigated for a water supply network in northern Louisiana which includes the Sparta aquifer. Runoff projections under climate change scenarios indicate that runoff will likely decrease in winter and increase in other seasons. Results from the developed conjunctive management model with MILFP indicate that the future reservoir water, even at 2.5% low inflow cumulative probability level, could counterbalance groundwater pumping reduction to satisfy demands while improving the Sparta aquifer through conditional groundwater head constraints.

© 2016 Elsevier B.V. All rights reserved.

1. Introduction

Sustainable planning and management of limited water resources has become a critical issue in light of decreasing water availability, increasing water demands, and imbalance use of surface water and groundwater. Water resources sustainability largely depends on proper management and efficient utilization of water (Fasakhodi et al., 2010). Conjunctive use of surface water and groundwater resources provides a long-term solution for improving water use efficiency (Singh, 2014).

However, managing future water resources often presents challenges due to uncertain future precipitation and runoff projections. Hydrometeorological variability is likely to increase in the near term (through 2050), leading to more intense, frequent climate events (Mahoney et al., 2012). Uncertainty and variability increases the complexity of the problems water resources decision makers face (Najafi et al., 2011). Due to the inherent uncertainty in modeling, it is very important to ensure the robustness of potentially expensive, irreversible adaptation decisions (Bastola et al., 2011).

Regional water resources undergoing climate change are typically studied through the modeling chain (Bosshard et al., 2013), which includes elements such as (1) global circulation models (GCMs), (2) future greenhouse gas emission (GHG) scenarios or representative concentration pathways (RCPs), (3) downscaling methods, and (4) hydrological models. Hydroclimate modeling can address (1) the impacts of future climate change, (2) the undefined effects of climate change on the availability of water resources, and (3) the resilience of water resources management (Bastola et al., 2011). The Intergovernmental Panel on Climate

☆ This manuscript has been co-authored by employees of Oak Ridge National Laboratory, managed by UT Battelle, LLC, under contract DE-AC05-00OR22725 with the U.S. Department of Energy. The United States Government retains and the publisher, by accepting the article for publication, acknowledges that the United States Government retains a non-exclusive, paid-up, irrevocable, world-wide license to publish or reproduce the published form of this manuscript, or allow others to do so, for United States Government purposes. The Department of Energy will provide public access to these results of federally sponsored research in accordance with the DOE Public Access Plan (http://energy.gov/downloads/doe-public-access-plan).

* Corresponding author.
E-mail addresses: amani1@lsu.edu (A. Mani), ftsai@lsu.edu (F.T.-C. Tsai), kaos@ornl.gov (S.-C. Kao), naz.bibi2007@gmail.com (B.S. Naz), mashfaq@ornl.gov (M. Ashfaq), rastogid@ornl.gov (D. Rastogi).

http://dx.doi.org/10.1016/j.jhydrol.2016.06.021
0022-1694/© 2016 Elsevier B.V. All rights reserved.

Change (IPCC) Fifth Assessment Report (AR5) suggested using multimodel ensembles for detection, attribution, impact, and adaptation studies (Stocker et al., 2010). It is evident that the uncertainty across different climate models is relatively larger than other sources of uncertainties (Weiland et al., 2012). Therefore, for water resources planning, the multimodel ensemble approach will be a more appropriate method than relying on a single model. Multimodel ensemble approaches exploit the diversity of multiple competent modeling chains and their advantages in describing hydrologic processes. This study adopts Bayesian model averaging (BMA) (Hoeting et al., 1999) as a multimodel ensemble method to account for projected inflow uncertainty for the conjunctive-use modeling under climate change projection uncertainty. BMA accounts for model uncertainty by producing a weighted probability density function using the posterior probability of each participating model while better performing predictions receive higher weights (Min et al., 2007; Liang et al., 2013). BMA has been applied to uncertainty analysis in weather forecasting and hydrologic prediction (Ajami et al., 2006; Duan et al., 2007; Min et al., 2007; Vrugt and Robinson, 2007; Zhang et al., 2009; Dong et al., 2013), and climate change impact analysis (Raftery and Zheng, 2003; Tebaldi et al., 2005; Buser et al., 2009; Smith et al., 2009; Liang et al., 2013).

Although projecting future runoff and quantifying its underlying uncertainty have been studied extensively in the literature, little work has been done to incorporate these results in future decision making for the conjunctive management of surface water and groundwater resources. Coupled simulation-optimization models have been used extensively for conjunctive management of groundwater and surface water resources, as indicated in the literature for complex water allocation problems. These coupled simulation-optimization models have aided in developing sustainable operational strategies (Mantoglou, 2003; Bhattacharjya and Datta, 2005; Ramesh and Mahesha, 2008; Bazargan-Lari et al., 2009; Mohammad Reazpour Tabari and Yazdi, 2014). For groundwater and multi-reservoir management, linear programming (LP), dynamic programming (DP), and genetic algorithm (GA) are the most commonly applied optimization approaches (Singh, 2012). Katsifarakis and Petala (2006) implemented both LP and differential evolution (DE) to manage a coastal karstic groundwater aquifer. Tamer Ayvaz and Karahan (2008) compared the performance of LP, NLP, DP, and GA in identifying unknown groundwater pumping well locations and pumping rates. The studies concluded that all optimization methods yield comparable results, while LP acquires the least computational expense and calculation time.

This study introduces a mixed integer linear fractional programming (MILFP) method for the conjunctive use of surface water and groundwater under uncertain future inflow projection. Fractional programming (FP) is the optimization of a ratio of two functions (Schaible, 1981). FP naturally addresses a multi-objective management problem by maximizing the benefit-cost ratio in water resources planning and management (Lara and Stancu-Minasian, 1999; Fasakhodi et al., 2010; Zhu and Huang, 2011; Ren et al., 2013; Guo et al., 2014). MILFP is a linear form of FP with integer decision variables, which optimizes the ratio of two mixed integer linear objective functions subject to mixed integer linear constraints. Due to its ability to be transformed to a mixed integer linear program (MILP), MILFP provides a computationally simple and efficient optimization framework to maximize one objective while minimizing its effect on resources through its ratio objective function.

In the following sections, MILFP is developed for a conjunctive-use study of surface water and groundwater for the Sparta aquifer in the northern Louisiana, USA. This study uses a hybrid downscaling method to develop future climate change scenarios based on 11 Coupled Model Intercomparison Project Phase 5 (CMIP5) GCMs. The downscaled precipitation and temperature are used as inputs to the Variable Infiltration Capacity (VIC) model (Liang et al., 1994) to project future natural runoff and reservoir inflow. The BMA is used to estimate the ensemble inflow to reservoirs. The projected demand withdrawals from reservoirs and groundwater pumping rates are then presented and discussed.

2. Methodology

2.1. Study area

The Sparta aquifer shown in Fig. 1a is the major source of water supply for Arkansas and northern Louisiana (McKee and Clark, 2003). From 1980 to 2010, the groundwater from the aquifer in northern Louisiana was withdrawn at a rate of 246,052–264,979 m^3/day, or ~65–70 million gallons per day (MGD) (Sargent, 2012). Over pumping has caused the groundwater level to decline by an average of 0.3–0.9 m/year (1–3 ft/year), and it has also caused saltwater intrusion (McKee and Clark, 2003). Areas with groundwater levels below the top of the Sparta aquifer are of particular concern (LaDNR, 2015). A wastewater treatment facility (Sparta Re-use Facility in West Monroe) was contructed to conserve the Sparta aquifer. Since 2013, the facility has offset groundwater pumping by ~18,927 m^3/day (5 MGD), providing reclaimed water to a major industrial user. Four reservoirs—Bayou D'Arbonne Lake, Lake Claiborne, Corney Lake, and Lake Bistineau (Fig. 1a)—supply fresh water to major cities in northern Louisiana (Meyer et al., 2002). These reservoirs are used primarily for recreation (US Army Corps of Engineers [USACE], 2015). Three reservoirs are located in the Bayou D'Arbonne subbasin (US Geological Survey [USGS] 8-digit hydrologic unit code [HUC8] 08040206), and another reservoir is in the Loggy Bayou subbasin (HUC8 – 11140203).

2.2. Conjunctive surface water and groundwater allocation model

To assess the effect of climate change on planning and management of reservoir operations and groundwater pumping, a conjunctive management model (Fig. 2) is developed based on fractional programming. It links a groundwater model and a hydrologic model. The objectives are to maximize groundwater withdrawal and to minimize reservoir storage deficit subject to a water balance equation for network flow, water demand constraints, and groundwater head constraints. Specifically, future reservoir inflow projections are derived from the VIC model given downscaled climate projections. BMA is adopted to derive ensemble mean and variance of reservoir inflows. Detailed information for the conjunctive management model is provided as follows.

The water supply network for northern Louisiana (Fig. 1b) includes six major cities: Farmerville (node D_1, Union Parish), Monroe (node D_2, including West Monroe in Ouachita Parish), Ruston (node D_3, Lincoln Parish), Arcadia (node D_4, Bienville Parish), Homer (node D_5, Claiborne Parish), and Minden (node D_6, Webster Parish). Their average monthly water demands are shown in Table 1 (Sargent, 2012). Farmerville and Monroe are designed to receive groundwater and surface water from Bayou D'Arbonne Lake (node S_2) located downstream from Corney Lake (node S_1) and Lake Claiborne (node S_3). The Sparta Re-use Facility has provided 18,927 m^3/day (5 MGD) to Monroe since 2013. Ruston is designed to receive groundwater and surface water from Bayou D'Arbonne Lake, Lake Claiborne (node S_3), and Lake Bistineau (node S_4). Arcadia, Minden, and Homer are near or in the recharge zone of the Sparta aquifer and are designed to use surface water only. The water demands and reclaimed water supply are assumed to be constant throughout the study.

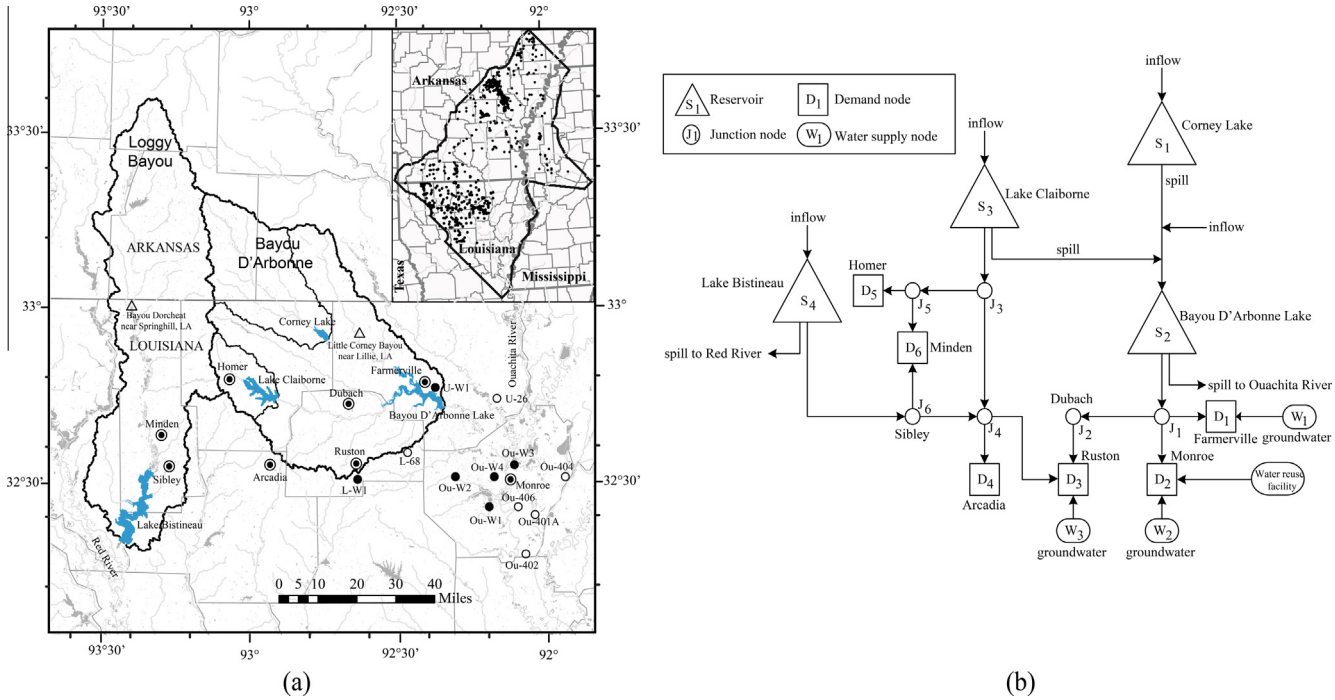

Fig. 1. (a) Areal extent of Sparta aquifer at top-right figure where solid circles are pumping wells (modified from McKee and Clark, 2003) and watershed boundaries for the four lakes. Open circles in the main map are USGS groundwater observation wells and open triangles are USGS streamflow gauges. Solid circles in the main map are selected pumping centers. (b) Proposed water supply network.

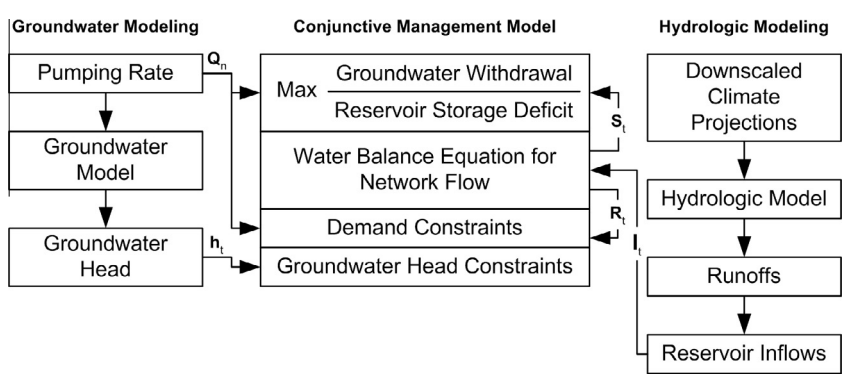

Fig. 2. Flowchart of the conjunctive management model.

Table 1
Water demands at demand nodes (Sargent, 2012).

City	Farmerville (D_1)	Monroe (D_2)	Ruston (D_3)	Arcadia (D_4)	Homer (D_5)	Minden (D_6)
Demand (m^3/day)	13,892	184,047	32,365	16,315	8858	26,763

Groundwater is mainly withdrawn from six major pumping centers (Fig. 1) located in Ouachita parish (four pumping centers for Monroe, node W_2), Union parish (one pumping center for Farmerville, node W_1) and Lincoln parish (one pumping center for Ruston, node W_3). Multiple USGS observation wells are shown Fig. 1a. To restore the Sparta aquifer to its predevelopment condition, this study assigns the 1975 groundwater level as the target groundwater level at four USGS observation wells in Ouachita, and it assigns 1985 groundwater level as the target level at one USGS observation well in Lincoln and another in Union. Pumping rates from other smaller wells in northern Louisiana are assumed to remain unchanged.

The network conjunctive water use model is simulated at monthly time steps. The maximum and minimum reservoir storages are the physical limits from the USACE National Dam Inventory (USACE, 2015). Not all reservoirs are regulated for high flow seasons due to their recreational use. No capacity limit is given to the arcs in the proposed water supply network. The lower bound of reservoir spill is assigned to be zero due to the lack of environmental flow information. Evaporation from reservoir surface and groundwater exchange along the reservoir boundaries is also assumed to be negligible due to lack of data.

2.3. Hydrologic modeling

To simulate the natural inflow to reservoirs, the semi-distributed VIC hydrologic model (Liang et al., 1994, 1996) is used.

VIC is a process-based hydrological model that simulates evapotranspiration, snow pack, surface runoff, baseflow, and other hydrologic mechanisms within a watershed. Within each grid cell, the water and energy balances are solved for multiple elevation bands and vegetation types, allowing the model to capture the subgrid variability of these land surface features. An external two-dimensional horizontal routing algorithm can then be used to estimate streamflow at a specified location (Lohmann et al., 1998). The VIC model is widely used for climate change impact assessment and can be used for either single basins (e.g., Christensen et al., 2004) or continental-scale studies (e.g., Vetter et al., 2015; Hagemann et al., 2013). However, it should also be noted that the current version of VIC model does not simulate groundwater.

Pre-organized VIC input data from Oubeidillah et al. (2014) are used to simulate surface hydrology for Bayou D'Arbonne (HUC8 – 08040206) and Loggy Bayou (HUC8 – 11140203) subbasins. The VIC model is implemented at 1/24° (~4 km) grid cell resolution with three-hour time steps. Five elevation bands are considered to incorporate the variability within the grids in precipitation and elevation. Based on the aggregated elevation from the National Elevation Dataset (NED) (Gesch et al., 2002) and also flow direction from the National Hydrography Dataset Plus (NHDPlus) (USEPA and USGS, 2010), flow direction grids in northern Louisiana are further generated for streamflow routing to the locations of reservoirs, and multiple USGS gauges. Oubeidillah et al. (2014) provide further details on VIC model setup, input parameters, and model calibration.

To evaluate the performance of VIC model, a control run simulation is conducted by using the Daymet dataset (Thornton et al., 1997) as the driving meteorological forcings. Both simulated total runoff (i.e., baseflow plus surface runoff) and routed streamflow were compared to the USGS WaterWatch runoff dataset (Brakebill et al., 2011) and the National Water Information System (NWIS) gauge observation (Fig. 3). In general, VIC-simulated total runoff for both subbasins shows strong similarity to the USGS WaterWatch runoff shown in Fig. 3a and b. Although runoff in the Loggy Bayou subbasin showed larger bias (NSE = 0.55), runoff in the Bayou D'Arbonne subbasin was well simulated (NSE = 0.80), suggesting that the overall surface water balance is reasonably simulated. Similarly, VIC-simulated streamflow at Bayou Dorcheat near Springhill, LA (in Loggy Bayou subbasin), and at Little Corney Bayou near Lillie, LA (in Bayou D'Arbonne subbasin), also match well with the observed streamflow shown in Fig. 3c and d. The locations of the two streamflow gauges are shown in Fig. 1a. The VIC model is then used to simulate the projected future reservoir inflow under multiple sets of future climate change projections (see Section 2.6).

2.4. Groundwater modeling

The USGS Sparta groundwater model (McKee and Clark, 2003) is adopted to simulate groundwater head in the Sparta aquifer from 1980 to 2010. Future pumping rates for 2011–2025 are assumed to be the same as 2010 pumping rates. McKee and Clark (2003) describes detailed model development. The monthly groundwater head is simulated, while the yearly groundwater pumping rates are optimized. This yields a 90 × 90 response matrix for the successive MILP problem. This study adopts the one-side finite difference method to calculate the sensitivities using 91 MODFLOW parallel runs on a supercomputer at Louisiana State University.

2.5. Fractional programming for conjunctive management

To balance the use between surface water from reservoirs and groundwater from pumping, a conjunctive management model is proposed based on fractional programming. The proposed conjunctive management model aims to maximize the ratio of two competing objectives, total groundwater withdrawal to the total deficit of reservoir storages with respect to their maximum storages. Because groundwater is generally cheaper and its quality is generally better than reservoir water, maximizing the ratio will maximize groundwater usage and minimize reservoir storage loss. This is especially important for reservoirs not used for flood control. To keep aquifers

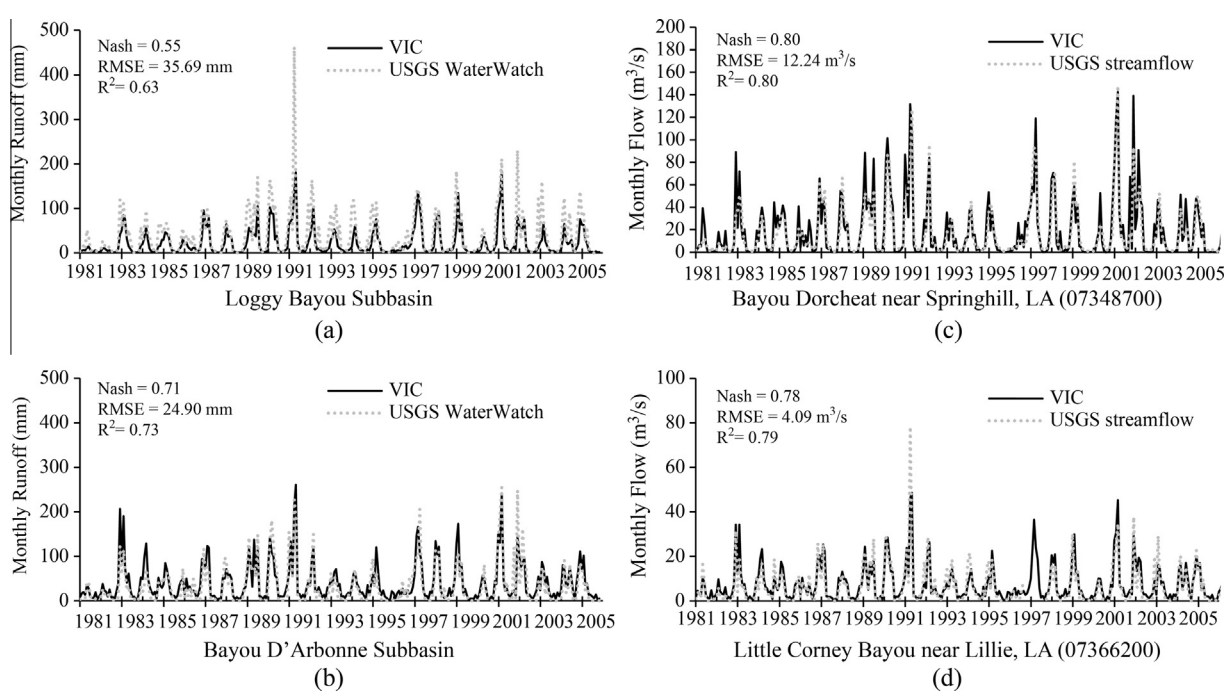

Fig. 3. Comparison of VIC simulated monthly runoff (mm) to USGS WaterWatch monthly runoff for (a) Loggy Bayou subbasin and (b) Bayou D'Arbonne subbasin. Comparison of VIC simulated monthly streamflow (m^3/s) to USGS streamflow at gauges (c) Bayou Dorcheat near Springhill, LA (Station Number: 07348700) and (d) Little Corney Bayou near Lillie, LA (Station Number: 07366200). NSE = Nash–Sutcliffe efficiency, RMSE = root mean square error, and R^2 = square of correlation coefficient.

for sustainable use, the study imposes groundwater head constraints at several control points, thus limiting groundwater withdrawal. The demand deficit caused by limiting groundwater pumping can be offset by using the reservoir water. The conjunctive management model is formulated as the following nonlinear fractional programming problem:

$$\text{Maximize } \frac{\sum_n \mathbf{1}^T \mathbf{Q}_n}{\sum_t \mathbf{1}^T (\mathbf{S}_{\max} - \mathbf{S}_t) + \beta}, \tag{1}$$

subject to

$$\begin{cases} \mathbf{h}_{t+1} \geqslant \mathbf{h}_t + \Delta_1 & \textit{if} \quad \mathbf{h}_t < \mathbf{h}^{\text{target}} \\ \mathbf{h}_{t+1} \geqslant \mathbf{h}_t - \Delta_2 & \textit{if} \quad \mathbf{h}_t \geqslant \mathbf{h}^{\text{target}} \end{cases}, \tag{2}$$

$$\mathbf{S}_{t+1} = \mathbf{S}_t + \mathbf{I}_t + \sum_{j \in \text{IN}} \mathbf{Sp}_t^{(j)} - \mathbf{R}_t - \mathbf{Sp}_t - \mathbf{E}_t, \tag{3}$$

$$\sum_{i \in \text{OUT}} \mathbf{x}_t^{(i)} - \sum_{j \in \text{IN}} \mathbf{x}_t^{(j)} = \mathbf{b}_t, \tag{4}$$

$$\mathbf{X}_{\min} \leqslant \mathbf{X} = [\mathbf{Q}_n, \mathbf{S}_t, \mathbf{R}_t, \mathbf{Sp}_t, \mathbf{x}_t]^T \leqslant \mathbf{X}_{\max}, \tag{5}$$

$$\mathbf{X}_{\min} = [\mathbf{Q}_{\min}, \mathbf{S}_{\min}, \mathbf{R}_{\min}, \mathbf{Sp}_{\min}, \mathbf{x}_{\min}]^T, \text{ and} \tag{6}$$

$$\mathbf{X}_{\max} = [\mathbf{Q}_{\max}, \mathbf{S}_{\max}, \mathbf{R}_{\max}, \mathbf{Sp}_{\max}, \mathbf{x}_{\max}]^T. \tag{7}$$

The vector $\mathbf{X}$ includes all state and decision variables:

$\mathbf{Q}_n$, the vector of groundwater pumping rate for different pumping wells during stress period n, $\mathbf{S}_t$, the vector of storage for different reservoirs at time t,

$\mathbf{R}_t$, the vector of demand withdrawal from different reservoirs during time period t, $\mathbf{Sp}_t$, the vector of spill from different reservoirs during time period t, and $\mathbf{x}_t$, the vector of water flow in a water supply network during time period t.

$\mathbf{X}_{\min}$ and $\mathbf{X}_{\max}$ are the vectors of the lower and upper bounds of the variables.

$\mathbf{h}_t$ is the vector of groundwater head at control locations at time t, which is a function of the pumping rate $\mathbf{Q}_n$.

$\mathbf{h}^{\text{target}}$ is the vector of target groundwater head at control locations.

Δ_1 and Δ_2 are the policy parameters, which are non-negative coefficients.

$\mathbf{I}_t$ is the vector of natural inflow to reservoirs during time period t.

$\mathbf{E}_t$ is the vector of evaporation from reservoir surface during time period t.

$\mathbf{b}_t$ is the source/sink nodes in the water supply network during time period t.

$\beta = 1$ is a non-negative constant to prevent the denominator value from being a very small number.

T is the transpose operator.

$\mathbf{1}$ is the vector of ones.

Each constraint is explained below. The nonlinearity is the result of constraint (2), where groundwater head is a nonlinear function of pumping rate.

2.5.1. Conditional head constraint

To avoid significant decline in groundwater levels, the conditional head constraint (2) is introduced with two non-negative coefficients,Δ_1 and Δ_2, as policy parameters to control groundwater levels around or above specified target levels at control locations. To handle constraint (2), a unit step function,

$$H(\mathbf{h}_t - \mathbf{h}^{\text{target}}) = 1, \text{ if } \mathbf{h}_t \geqslant \mathbf{h}^{\text{target}}; 0, \text{ otherwise}, \tag{8}$$

is introduced to make the conditional head constraint more concise:

$$\mathbf{h}_{t+1} - \mathbf{h}_t + (\Delta_1 + \Delta_2) H(\mathbf{h}_t - \mathbf{h}^{\text{target}}) \geqslant \Delta_1. \tag{9}$$

This conditional constraint is especially suitable for managing depleting aquifers since it enforces groundwater level increase at least Δ_1 units for the next time step if current groundwater level is lower than the specified target level; otherwise, it allows groundwater level to decrease up to Δ_2 units for the next time step. Δ_1 and Δ_2 values are subject to analysts' choice. $\Delta_1 = 0.305$ m (1 ft) and $\Delta_2 = 0.610$ m (2 ft) were assigned in Eq. (2) for this study since they made target heads at selected observation wells achievable in a 15-year period. Moreover, the coefficient values avoid high groundwater level fluctuations over time.

Directly dealing with constraint (9) in the optimization problem is not straightforward. In Appendix A, this study introduces an equivalent set of mixed-integer nonlinear constraints to represent constraint (9). By using the first-order Taylor series expansion to linearize groundwater head with respect to pumping rate, the conditional head constraint (9) is ultimately replaced by a set of mixed-integer linear constraints.

2.5.2. Water balance equation at reservoirs

Eq. (3) is the water balance equation at reservoirs. The term $\sum_{j \in \text{IN}} \mathbf{Sp}_t^{(j)}$ is the total spill from upstream reservoirs during time period t. The USGS gauge record indicates that the initial reservoir storages were full at the beginning of 2011. The VIC hydrologic model, driven by the downscaled temperature and precipitation from 11 ensemble members of future climate change projections, was used to simulate the natural inflow $\mathbf{I}_t$ entering the reservoirs. The development of future reservoir inflow scenarios is discussed further in the later sections.

2.5.3. Water supply network

Eq. (4) is the water balance equation at junction and demand nodes in a water supply network given that reservoirs are the source of surface water and pumping wells are the source of groundwater to the demand nodes. $\sum_{i \in \text{OUT}} \mathbf{x}_t^{(i)}$ is the total outflow and $\sum_{j \in \text{IN}} \mathbf{x}_t^{(j)}$ is the total inflow for each node. For a junction node that diverts water to other nodes, $\mathbf{b}_t$ is zero. For a demand node, the total inflow is the sum of surface water and groundwater, the total outflow is zero, and $\mathbf{b}_t$ is water demand (negative value).

2.5.4. Transformation to successive MILP

Following Appendix A, a successive MILFP problem is formulated. Further transformation is conducted in Appendix B to transform the successive MILFP problem into a successive mixed-integer linear programming (MILP) problem by the Charnes-Cooper transformation technique (Charnes and Cooper, 1962). This study terminates the successive procedure when the sum of absolute head differences at control locations between iterations is less than a threshold, i.e.,

$$\|\mathbf{h}_t\left(\mathbf{Q}_n^{k+1}\right) - \mathbf{h}_t\left(\mathbf{Q}_n^{k}\right)\|_1 \leqslant \eta, \tag{10}$$

where $\|\cdot\|_1$ is the 1-norm, and η is the convergence threshold. For a 15-year network flow optimization, the successive MILFP problem has 4320 decision variables and 8190 constraints. After transformation, the successive MILP problem has 4321 decision variables and 8551 constraints. The IBM ILOG CPLEX Optimizer (IBM, 2009) is used to solve the MILP problem.

2.6. Future hydroclimate projections

A hybrid downscaling method (i.e., both dynamical and statistical) is used in this study to develop possible future climate change

projections based on the CMIP5 GCM outputs. The coarser resolution GCM outputs (~150 km) are first dynamically downscaled to 18 km resolution using the International Centre for Theoretical Physics Regional Climate Model version 4 (RegCM4) (Giorgi et al., 2012). The RegCM4-simulated temperature and precipitation are then statistically interpolated and bias-corrected to 1/24° (~4 km) resolution for the follow-up hydrologic simulation. This study selects 11 CMIP5 GCMs under the Representative Concentration Pathway (RCP) 8.5 emission scenario (ACCESS1-0, BCC-CSM1-1, CCSM4, CMCC-CM, FGOALS-G2, GFDL-ESM2M, IPSL-CM5A-LR, MIROC5, MPI-ESM-MR, MRI-CGCM3, and Nor-ESM1-M). This hybrid downscaling approach has been described in several recent hydroclimate studies (Ashfaq et al., 2010, 2013).

For dynamical downscaling, RegCM4 is forced at its lateral and lower boundaries every 6 h using atmospheric and sea-surface temperature fields from the GCMs. The RegCM4 simulations are carried out at 18 km horizontal grid spacing with 18 vertical levels that cover a domain similar to Diffenbaugh et al. (2011). Each set of experiments consists of 41 years in the baseline (1965–2005) and 41 years in the near future (2010–2050) periods with the first year disregarded for model spin up.

While there are over 50 GCMs contributed to CMIP5, only less than one-third archived three-dimensional atmospheric fields at a sub-daily timescale, which is necessary for dynamical downscaling. Therefore, the selection of GCMs in this study is mainly based on data availability. After balancing the resource limitation and the need of multimodel projections, 11 ensemble members—one from each different CMIP5 GCM—are selected in this study. The RCP 8.5 scenario is selected because it is closest to the current observed trajectory. The performance and skills of each selected GCM are not specifically evaluated in this study.

After RegCM4 simulation, the 18 km daily precipitation and maximum/minimum surface temperatures are statistically interpolated and bias corrected to 1/24° (~4 km) resolution using a quantile-based bias correction method (Ashfaq et al., 2010, 2013). The 1/24° (~4 km) resolution 1966–2005 monthly precipitation and temperature from the Parameter-elevation Regressions on Independent Slopes Model (PRISM) (Daly et al., 2008) are used as the historic observation for bias correction. Since most hydrologic models are highly sensitive to minor variations in meteorological forcings, several studies have suggested that statistical bias correction should be performed for the dynamically downscaled precipitation and temperature before conducting hydrologic simulation for better accuracy and lower bias (Rojas et al., 2011; Ahmed et al., 2013).

2.7. Reservoir inflow projection by Bayesian model averaging

Driven by the downscaled temperature and precipitation, the VIC model is used to simulate an ensemble of 11 sets of baseline (1966–2005) and future (2011–2050) runoff and streamflow projections. While all dynamically downscaled precipitation and temperature have been bias-corrected by PRISM (i.e., having climatological averages similar to PRISM), the VIC-simulated runoff and streamflow during the baseline period can still vary due to differences in the interannual variability of precipitation and temperature of each ensemble member. Therefore, instead of assigning equal weight to each model, this study adopts the Bayesian model averaging approach to derive an average runoff projection from multiple sets of reservoir inflow projections. Higher weights are assigned to climate models that produce more similar interannual runoff variability to the USGS WaterWatch runoff.

Inflows have been considered to follow a lognormal distribution (Vogel and Stedinger, 1987; Vogel et al., 1999). In this study, BMA is used to calculate mean reservoir log-inflow projection as follows:

$$\overline{\mathbf{Y}}_t(\mathbf{D}) = \sum_p \overline{\mathbf{Y}}_t(\mathbf{D}, M_p) Pr(M_p|\mathbf{D}), \tag{11}$$

where $\mathbf{Y}_t = \ln(\mathbf{I}_t)$ is the vector of natural logarithms of reservoir inflows,

$\overline{\mathbf{Y}}_t(\mathbf{D})$ is the vector of mean reservoir projected log-inflows at time t given data $\mathbf{D}$,

$\overline{\mathbf{Y}}_t(\mathbf{D}, M_p)$ is the vector of mean reservoir projected log-inflows by hydroclimate model M_p, at time t given data $\mathbf{D}$, and

$Pr(M_p|\mathbf{D})$ is the posterior model probability for the hydroclimate model M_p, which is the model weight for the hydroclimate model M_p. The variances of the reservoir projected log-inflows are as follows:

$$\sigma^2(\mathbf{Y}_t|\mathbf{D}) = \sum_p \sigma^2(\mathbf{Y}_t|\mathbf{D}, M_p) Pr(M_p|\mathbf{D}) + \sum_p \left(\overline{\mathbf{Y}}_t(\mathbf{D}, M_p) - \overline{\mathbf{Y}}_t(\mathbf{D})\right)^2 Pr(M_p|\mathbf{D}), \tag{12}$$

where $\sigma^2(\mathbf{Y}_t|\mathbf{D}, M_p)$ are the log-inflow variances using the hydroclimate model M_p. The internal uncertainty of individual hydroclimate models creates the first term in Eq. (12). The mean inflow projection uncertainty using different hydroclimate models creates the second term in Eq. (12).

Calculating $\overline{\mathbf{Y}}_t(\mathbf{D}, M_p)$ can be challenging if full model parameter range of hydroclimate model M_p is taken into account. Following the suggestion of Draper (1995), $\overline{\mathbf{Y}}_t(\mathbf{D}, M_p)$ is approximated by $\mathbf{Y}_t(\mathbf{D}, \hat{\boldsymbol{\beta}}_p, M_p)$, where $\hat{\boldsymbol{\beta}}_p$ is the maximum likelihood estimate of model parameters $\hat{\boldsymbol{\beta}}_p$ of the hydroclimate model M_p. Therefore, $\overline{\mathbf{Y}}_t(\mathbf{D}, M_p)$ is approximated by the log-runoff output of the calibrated VIC model with climate forcing from a GCM.

Calculating the model weight $Pr(M_p|\mathbf{D})$ is another challenging task due to the calculation of the marginal likelihood in the Bayes' theorem. Many studies have contributed to the discussions of how $Pr(M_p|\mathbf{D})$ be calculated. This study does not elaborate on these discussions, but simply adopts the Bayesian information criterion (Schwarz, 1978) and the variance window (Tsai and Li, 2008) to approximate the marginal likelihood function. The Bayesian information criterion (BIC) is

$$\mathrm{BIC}_p = \sum_i \frac{\left(\ln\ Q_{p,i} - \ln\ Q_i^{\mathrm{obs}}\right)^2}{\sigma_{p,i}^2} + N\ \ln\ 2\pi + k_p\ \ln\ (N), \tag{13}$$

where

$\ln\ Q_{p,i}$ is the ith log-runoff projected by the hydroclimate model M_p,

$\ln\ Q_i^{\mathrm{obs}}$ is the ith USGS WaterWatch runoff data,

$\sigma_{p,i}^2$ is the error variance for the ith runoff data,

N is the number runoff data, and k_p is the number of unknown model parameters. The model weight can be approximated by the following equation:

$$Pr(M_p|\mathbf{D}) \approx \frac{\exp\left(-\frac{1}{2}\alpha(\mathrm{BIC}_p - \mathrm{BIC}_{\min})\right)}{\sum_q \exp\left(-\frac{1}{2}\alpha(\mathrm{BIC}_q - \mathrm{BIC}_{\min})\right)}, \tag{14}$$

where α is the scaling factor, and $\mathrm{BIC}_{\min}$ is the minimum BIC value of all hydroclimate models. Tsai and Li (2008) provide the details on implementation. Climate models that produce interannual runoff variability similar to the USGS WaterWatch log-runoffs will have smaller BIC values and higher model weights.

3. Results and discussion

3.1. Comparison with other CMIP5 models

Since the adopted hydroclimate ensemble was restricted to 11 GCMs, their relative change compared to other CMIP5 members was evaluated (Fig. 4). RegCM-RCP8.5 represents the 11 downscaled models used in this study. A total of 97 statistically downscaled climate projections under four emission scenarios (RCPs 2.6, 4.5, 6.0, and 8.5) are obtained from the bias correction spatial disaggregation (BCSD) data archive (Brekke et al., 2013). The average annual percentage change of precipitation and the degree change of temperature from the 1966–2005 baseline to the 2011–2050 near future period in the study area are calculated. The ensemble median of the 97 BCSD downscaled projections is marked by a dashed line (Fig. 4). All models project a consistent increase in temperature ranging from +0.5 °C to ~+2.5 °C, and −15% to +20% change in precipitation is projected with relatively large intermodel variability. In terms of the multimodel median, the 11 climate projections used in this study are around −0.5 °C cooler and +5% wetter than the BCSD in the study area. Although the highest emission scenario is chosen, the 11 simulations are not biased toward the warming side. This is because the difference among various emission scenarios only becomes significant after 2030 (Peters et al., 2013), so climate variability remains the main governing factor in the near-term 21st century projection period.

3.2. Runoff projections under climate change scenarios

Changes in near future seasonal runoffs (2011–2049) projected by different hydroclimate ensemble members with respect to the historical seasonal WaterWatch runoffs (1980–2005) for Bayou D'Arbonne subbasin were shown in Table 2. These changes indicate a decrease in near future runoff in winter (DJF). This is consistent with other studies (Seager et al., 2013; Milly et al., 2005; Mulholland et al., 1997) that projected an overall decrease in mean runoff for the southern region of the US; however, the decrease would be greater than 10% in this region. On the other hand, near future runoff would increase in summer (JJA) and fall (SON) significantly. Near future runoff is likely to increase in spring (MAM). Although not shown here, similar near future runoff changes were also obtained for Loggy Bayou subbasin. The near future mean annual runoffs due to different GCMs could decrease by 180.74 mm, or they could increase by 90.75 mm in Loggy Bayou subbasin as compared to the historical mean annual runoffs, and there could be a 164.58 mm decrease and 133.11 mm increase in Bayou D'Arbonne subbasin. The hydroclimate modeling results show considerable spread of possible future outcomes.

The model weights for the hydroclimate ensembles were obtained based on their similar interannual variability to the USGS WaterWatch log-runoffs for the subbasins during 1980–2005 (14). The probability plot shown in Fig. 5 indicates that the monthly runoffs can be reasonably assumed to be log normally distributed. As

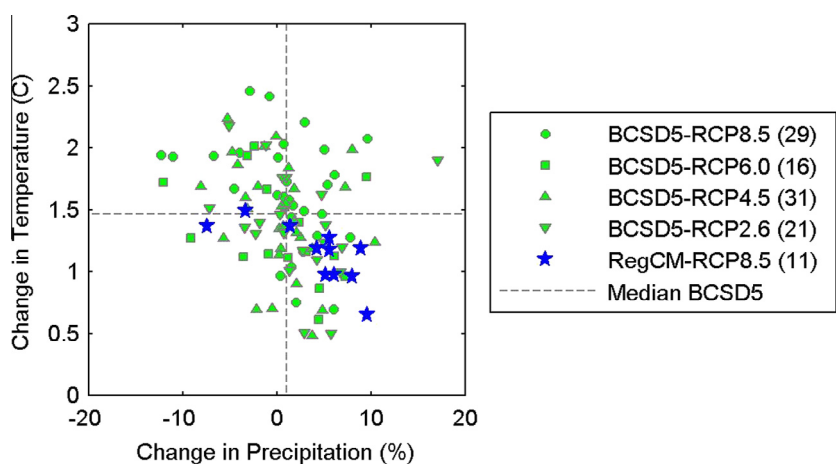

Fig. 4. Scatter plots of projected mean annual temperature and precipitation changes for 97 statistically downscaled CMIP5 GCM projections (BCSD) under four emission scenarios (RCP 2.6, 4.5, 6.0, and 8.5; green symbols) and the 11 RegCM4 simulations (blue symbols) used in this study. Change is defined as the degree change of average temperature (C) and percentage change of average precipitation (%) from 1966–2005 baseline to 2011–2050 future periods in the study area. The 97 climate projections were obtained from the BCSD data archive (Brekke et al., 2013). (For interpretation of the references to colour in this figure legend, the reader is referred to the web version of this article.)

Table 2
Future seasonal runoff changes (2011–2049) in the Bayou D'Arbonne subbasin (HUC8 – 08040206) compared to the USGS WaterWatch runoff (1980–2005).

Model name	Change in average runoff (%)				Change in median runoff (%)			
	DJF	MAM	JJA	SON	DJF	MAM	JJA	SON
ACCESS1-0	−53.1	−1.9	12.0	25.8	−67.0	−3.3	14.5	16.4
BCC-CSM1-1	−25.3	18.3	12.2	36.7	−52.6	32.2	17.1	19.3
CCSM4	−32.7	68.1	19.2	24.2	−75.8	91.1	29.4	19.5
CMCC-CM	−11.2	16.4	24.3	29.1	−23.4	32.3	28.2	29.3
FGOALS-G2	−112.2	−52.6	17.7	0.9	−134.4	−28.5	33.3	7.9
GFDL-ESM2M	28.1	11.0	13.7	17.8	−8.3	13.6	19.2	15.2
IPSL-CM5A-LR	6.9	30.5	19.4	25.0	6.2	46.9	25.4	29.5
MIROC5	−53.1	9.2	26.4	24.5	−68.4	19.3	29.9	33.9
MPI-ESM-MR	22.4	5.8	15.9	23.6	16.4	22.0	27.0	22.6
MRI-CGCM3	−0.1	44.3	28.8	19.0	−14.3	46.8	32.2	22.2
Nor-ESM1-M	−41.6	−25.8	16.6	14.3	−45.6	−25.9	30.2	14.5
BMA	−19.3	42.6	20.4	29.1	−47.6	57.2	34.2	29.5

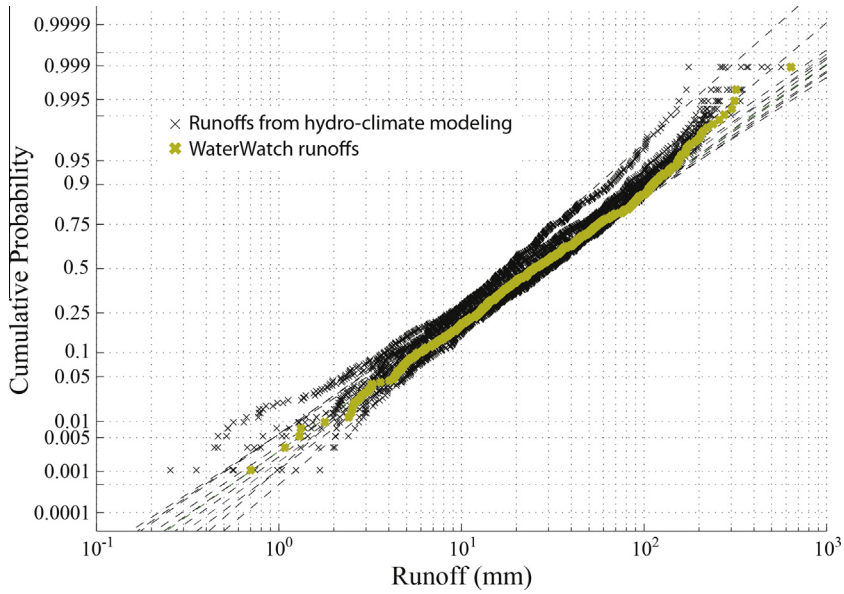

Fig. 5. Cumulative probability of simulated runoff from 11 hydro-climate models and the USGS WaterWatch data in 1980–2005.

Table 3
Model weights and BIC values based on their similarity of interannual runoff variability to the USGS WaterWatch dataset during the historical period (1980–2005).

Model name	Ensemble member	Model weights	BIC
ACCESS1-0	r1p1i1	0.072	597.61
BCC-CSM1-1	r1p1i1	0.127	578.68
CCSM4	r6p1i1	0.461	535.86
CMCC-CM	r1p1i1	0.011	661.05
FGOALS-G2	r1p1i1	0.038	619.09
GFDL-ESM2M	r1p1i1	0.032	624.11
IPSL-CM5A-LR	r1p1i1	0.020	640.70
MIROC5	r1p1i1	0.086	591.57
MPI-ESM-MR	r1p1i1	0.001	728.84
MRI-CGCM3	r1p1i1	0.004	690.75
Nor-ESM1-M	r1p1i1	0.148	573.74

shown in Table 3, RegCM4-CCSM4 has the highest similarity to WaterWatch log-runoffs, and RegCM4-MPI-ESM-MR has the least similarity. BMA means of log-runoffs were obtained by using Eq. (11), and log runoffs were obtained by using Eq. (12) to determine 95% confidence interval. After back-transformation, most of the USGS WaterWatch runoffs are within the 95% confidence interval as shown Fig. 6a and b for the historical period.

The BMA means and the 95% confidence interval of near future runoffs are shown in Fig. 6c and d. The results indicate high runoff projection uncertainty in years 2017, 2019, 2023 and 2024. By comparing with the average annual runoff of the historical period, the BMA results indicate an increase of 66.95 mm/year for Bayou D'Arbonne subbasin and an increase of 61.89 mm/year for Loggy Bayou subbasin in the near future period. This is contrary to the previous findings (Seager et al., 2013; Milly et al., 2005; Mulholland et al., 1997) that projected runoff decrease in the US southern region.

3.3. Inflow projections under climate change scenarios

Future monthly inflows to Lake Bistineau were estimated the same as the runoffs for Loggy Bayou subbasin (Fig. 6c). Future monthly inflows to Bayou D'Arbonne Lake, Lake Claiborne, and Corney Lake were calculated from the fractional runoffs of Bayou D'Arbonne subbasin (see Fig. 6d) based on the ratios of their drainage areas to those in the Bayou D'Arbonne subbasin area. The watershed areas shown in Fig. 1a are 4157 km^2 for Bayou D'Arbonne Lake, 334 km^2 for Lake Claiborne, 1109 km^2 for Corney Lake, and 3768 km^2 for Lake Bistineau. Based on the BMA means and variances of log-runoffs under the Gaussian assumption, this study investigates the optimized conjunctive management solutions under the future low inflow projections at 50%, 10%, and 2.5% cumulative probability level as shown in Fig. 7.

3.4. Impact of conjunctive use on reservoirs

Noticeable deficits in the reservoir storages would be produced at the 2.5% low inflow, as shown in Fig. 8. The storage capacity of Corney Lake is relatively very small and is not shown here. Over the 15-year span (2011–2025), Corney Lake would lose 18 million m^3 (4612 MG) in storage, Bayou D'Arbonne Lake would lose 4547 million m^3 (1,201,123 MG), Lake Claiborne would lose 899 million m^3 (237,557 MG), and Lake Bistineau would lose 1954 million m^3 (516,071 MG). Storage would decrease significantly at Lakes Claiborne and Bistineau starting in the summer of 2023 because the 2.5% low inflow would not be able to meet demands without significantly using storages. Storage loss would not be noticeable at the 10% and 50% cumulative low inflow probability levels.

Low inflows would result in low spills from the reservoirs, as shown in Fig. 9. For the 2.5% low inflow, Bayou D'Arbonne Lake would spill only 0.94% of its annual inflows on average to Ouachita River. Lake Bistineau would spill only 2.55% of its annual inflows on average to Red River. These low spills might not be favorable to environmental flows in some months during 2011–2025. However, the 50% low inflows would allow Bayou D'Arbonne Lake to spill 60.29% of its annual inflows on average to the Ouachita River. Lake Bistineau would spill 56.7% of its annual inflows on average to Red River. These high spills would satisfy environmental flows.

3.5. Impact of conjunctive use on sparta aquifer

Due to sufficient surface water (inflows plus reservoir storages) to meet water demand in 2011–2025, the same optimized groundwater pumping rates resulted, regardless of considering 2.5%, 10%, or 50% low inflow (Fig. 10). The annual mean of future optimized pumpage for pumping center Ou-W1 would decrease by 45.55%,

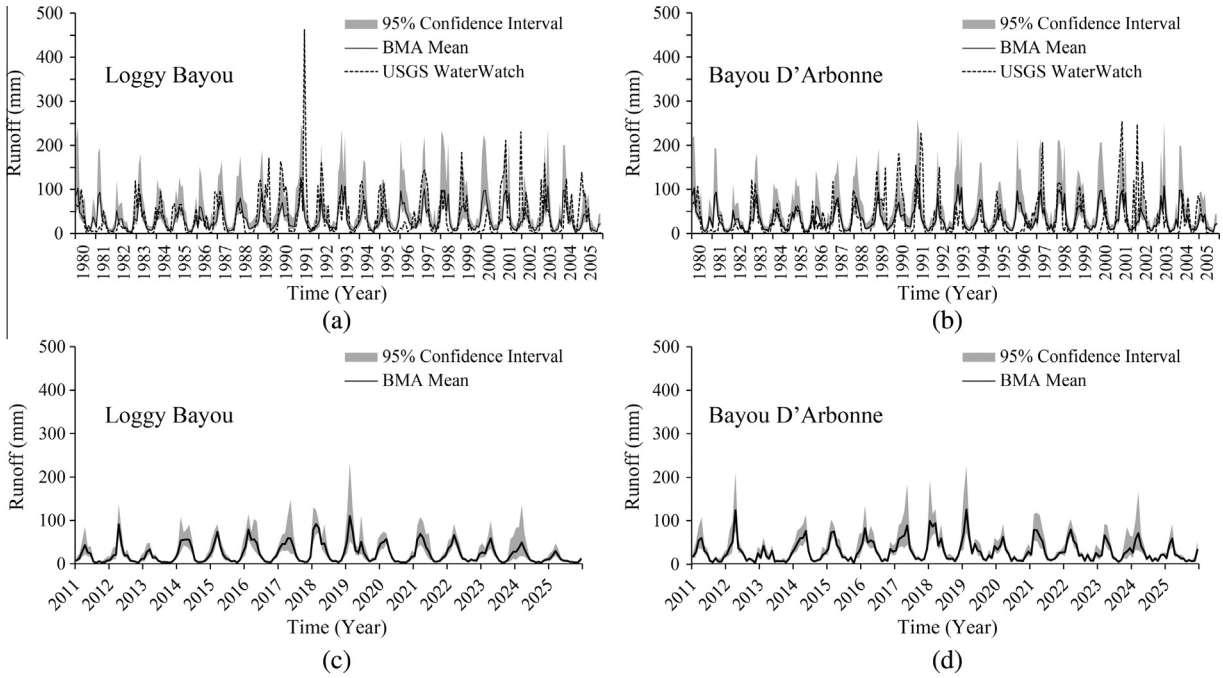

Fig. 6. BMA mean monthly runoff (mm) and 95% confidence interval for (a) Loggy Bayou subbasin, (b) Bayou D'Arbonne subbasin for historical period (1980–2005), (c) Loggy Bayou subbasin, and (d) Bayou D'Arbonne subbasin for future period (2011–2025).

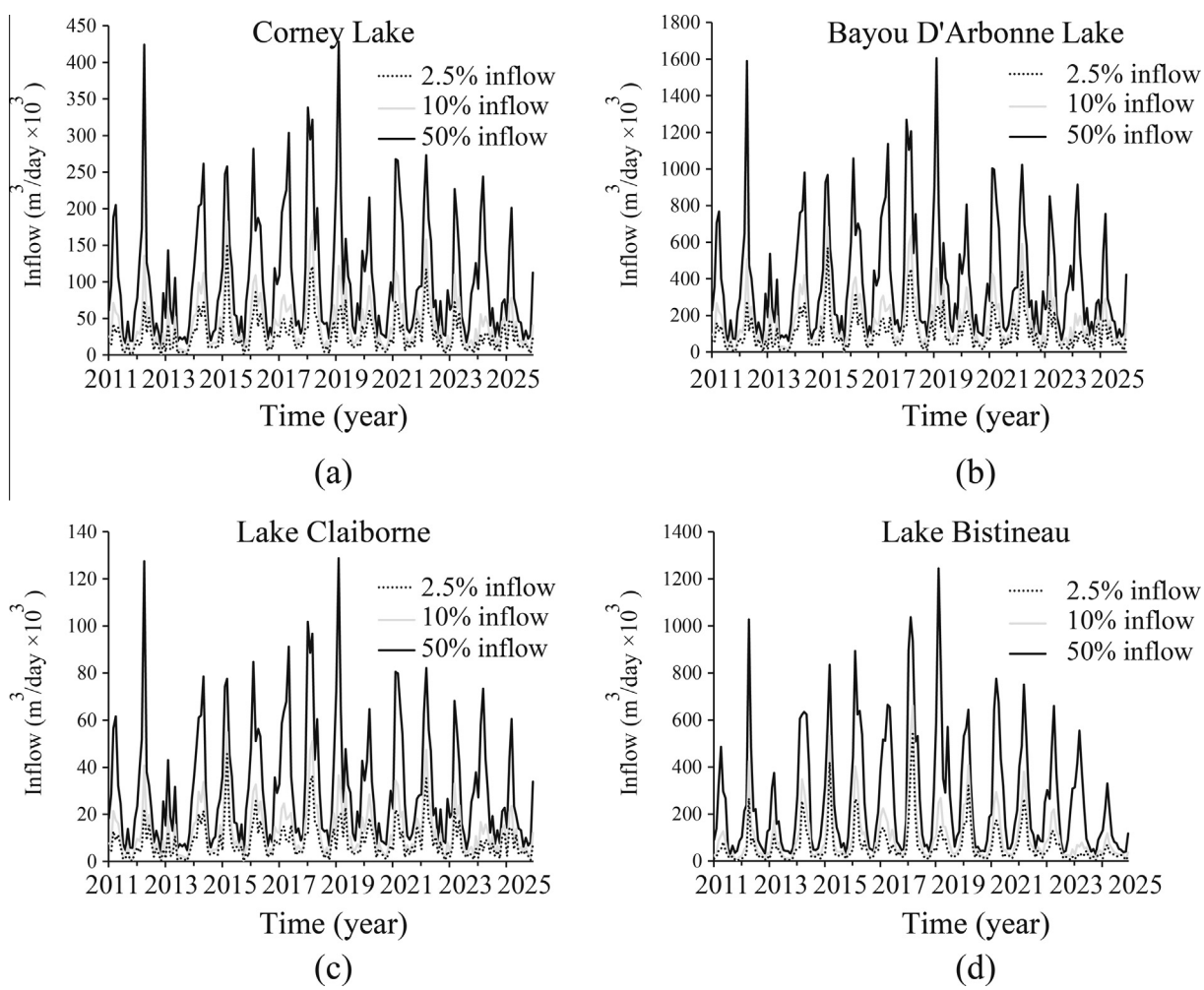

Fig. 7. Low inflow projections at 2.5%, 10%, and 50% cumulative probability levels for (a) Corney Lake, (b) Bayou D'Arbonne Lake, (c) Lake Claiborne, and (d) Lake Bistineau for future period (2011–2025).

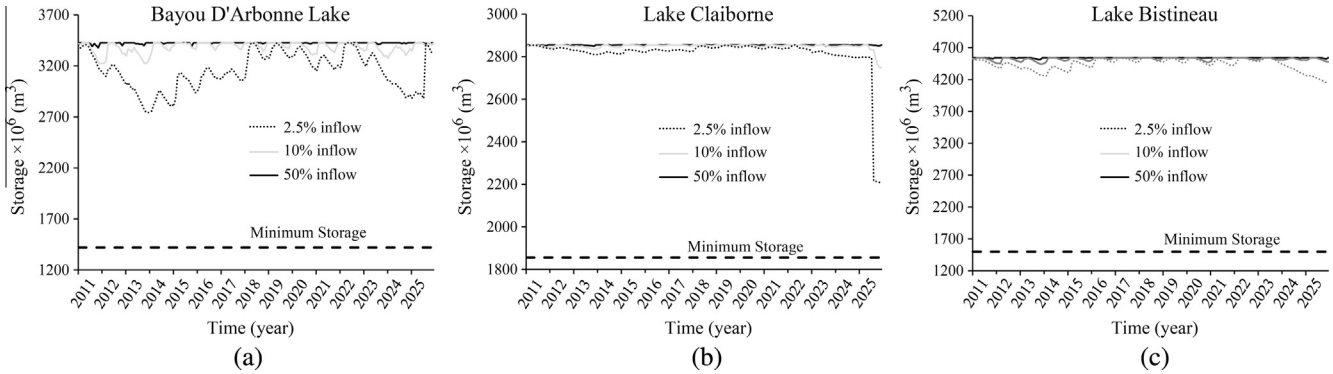

Fig. 8. Optimized storage distributions with 2.5%, 10%, and 50% low inflow projections for future period (2011–2025).

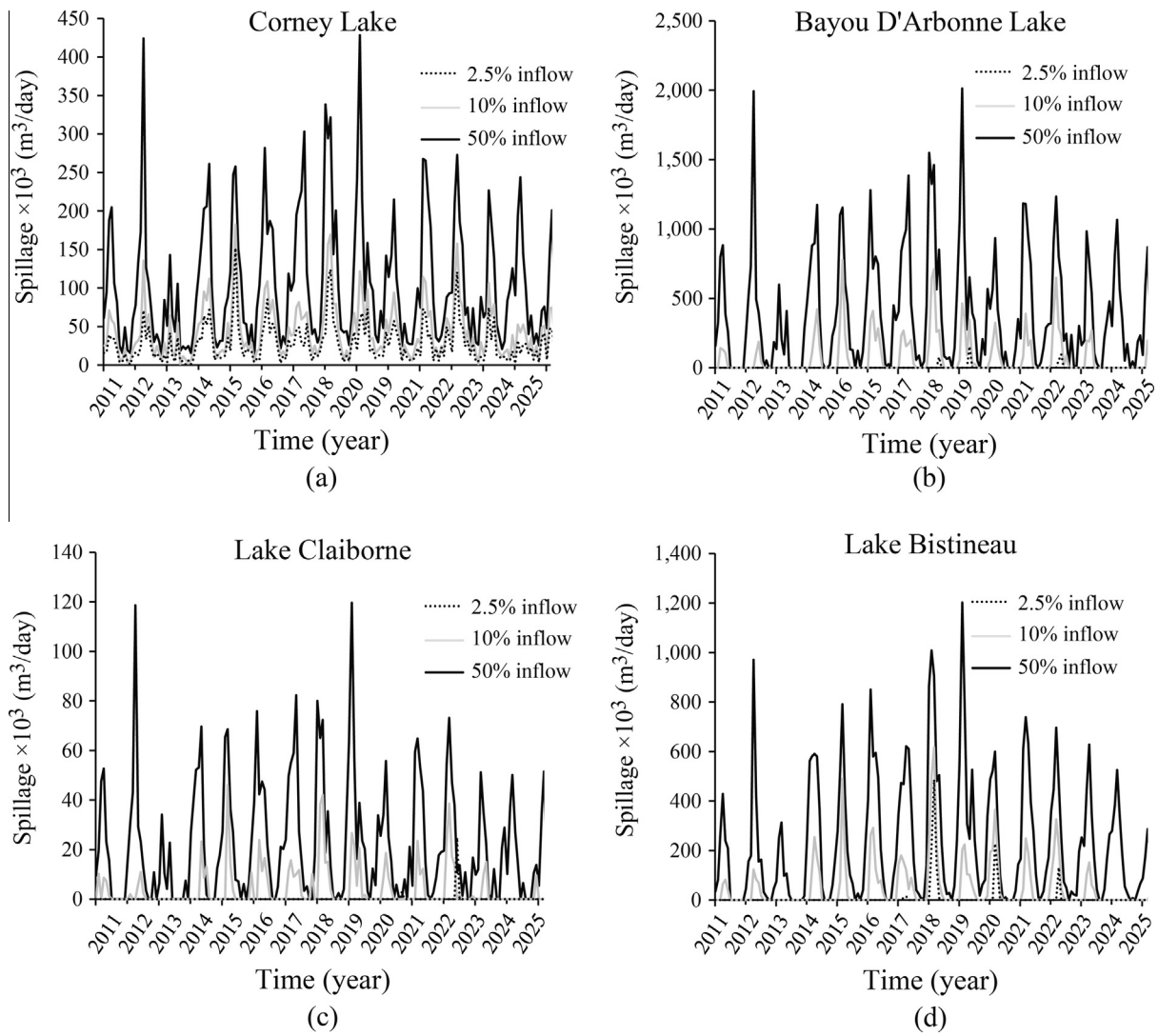

Fig. 9. Optimized spills from the four reservoirs for future period (2011–2025).

and at Ou-W2 it would decrease by 99.22% as compared to decreases in 2001–2010. However, the annual mean of future optimized pumpage for pumping center Ou-W3 would increase by 18.62%, and Ou-W4 it would increase by 20.55%. Overall, conjunctive management shows that the annual mean pumpage in Ouachita would decrease from 2,4491,614 m^3/day (6470 MGD from 2001 to 2010) to 18,029,916 m^3/day (4763 MGD from 2011 to 2025), a 26.38% reduction. This could be offset by the surface water. The annual mean of optimized pumpage at L-W1 in Lincoln would decrease by 19.41% as compared to the decreases in 2001–2010. The annual mean of optimized pumpage at U-W1 in Union would increase by 195.77%.

Using $\Delta_1 = 0.305$ m (1 ft) and $\Delta_2 = 0.610$ m (2 ft) in Eq. (2), as shown in Fig. 11, groundwater levels at the selected control points

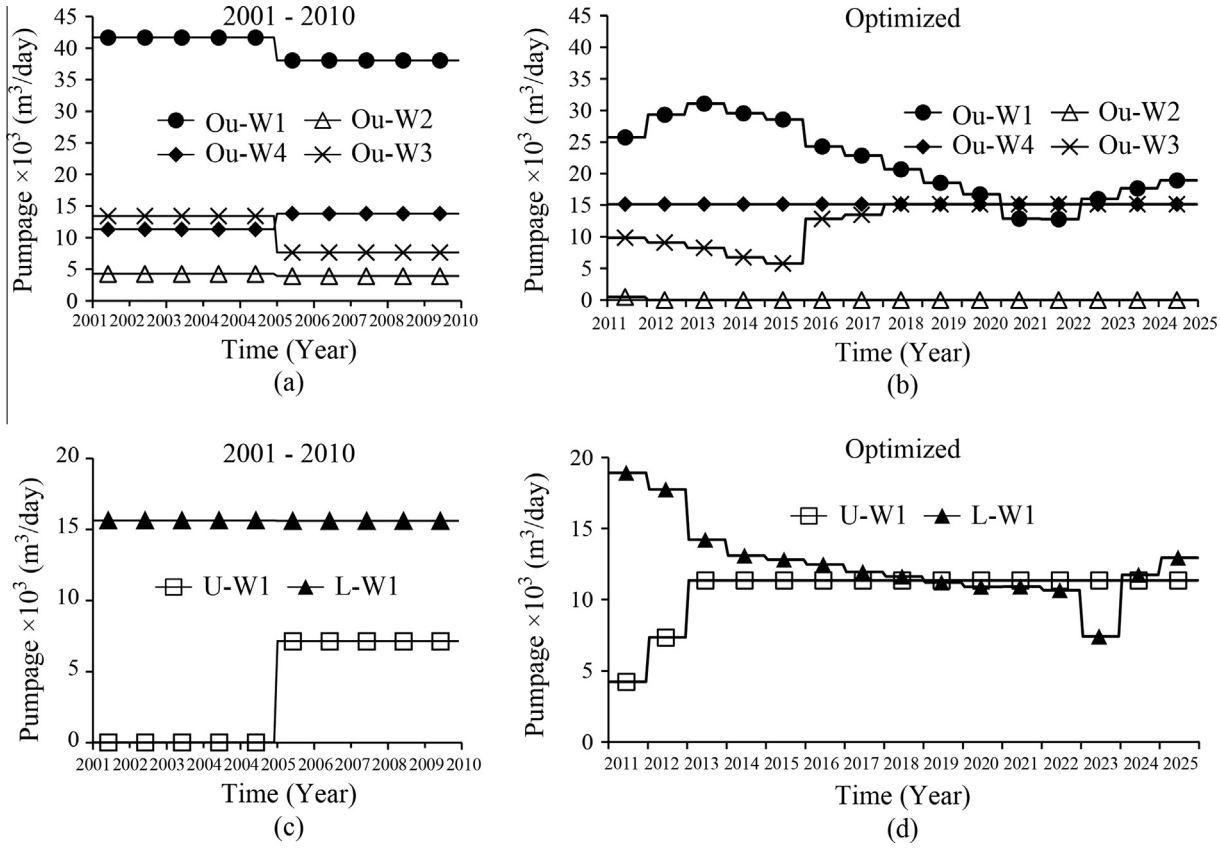

Fig. 10. Pumping rates for Ouachita wells (a) for 2001–2010 and (b) 2011–2025 optimized. Pumping rates for Union and Lincoln wells (c) for 2001–2010 and (d) 2011–2025 optimized.

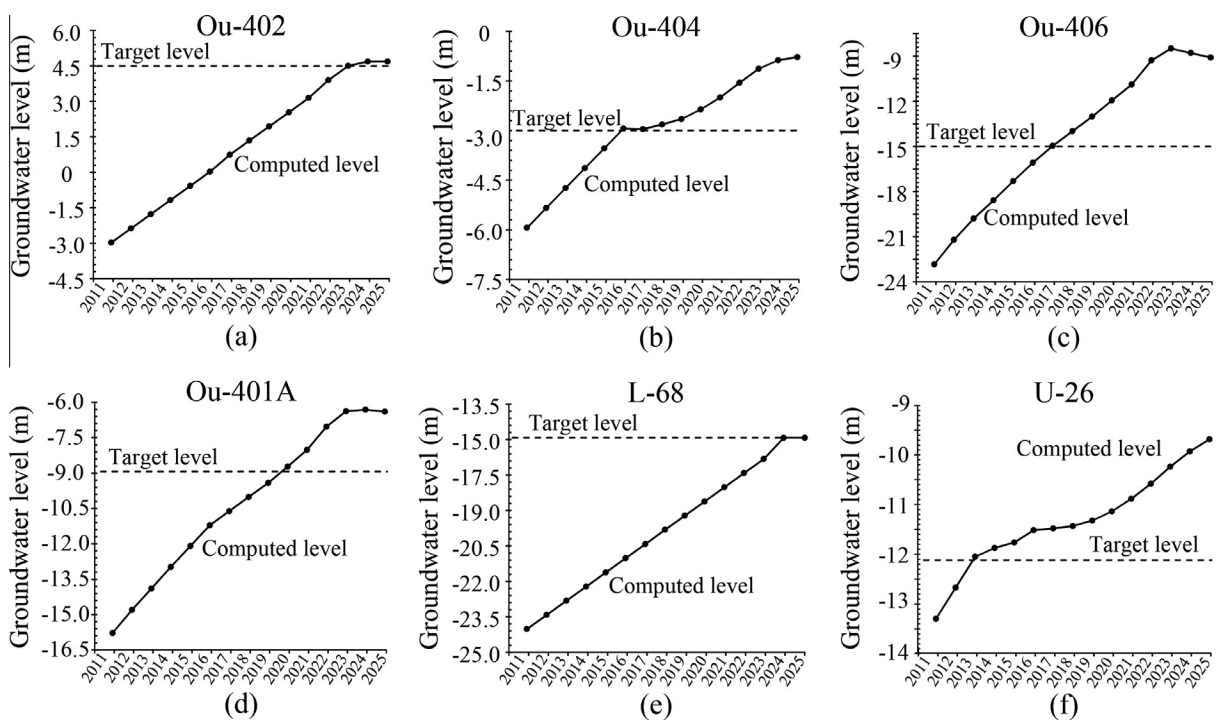

Fig. 11. Groundwater levels (m) above NGVD 1929 at six selected USGS wells for future period (2011–2025).

would reach or pass their target levels by 2025. By significantly reducing pumpage in Ouachita, groundwater level at U-26 would still increase even though the pumping rate increases for U-W1. In summary, the target groundwater levels could be achieved by only decreasing 13,703 m^3/day (3.62 MGD) from the annual mean pumpage during 2001–2010. This pumpage reduction is

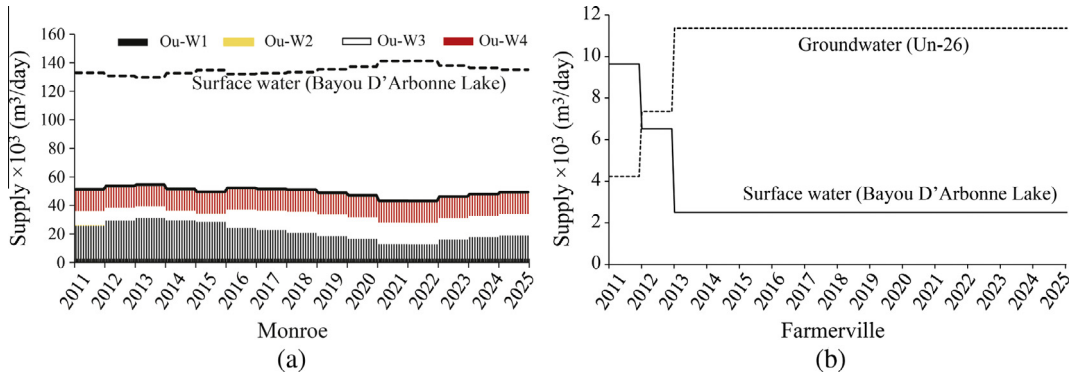

Fig. 12. Optimized surface water and groundwater supplies given 2.5%, 10%, and 50% low inflow projections for (a) Monroe (water re-use supply in West Monroe is subtracted from the total demand) and (b) Farmerville.

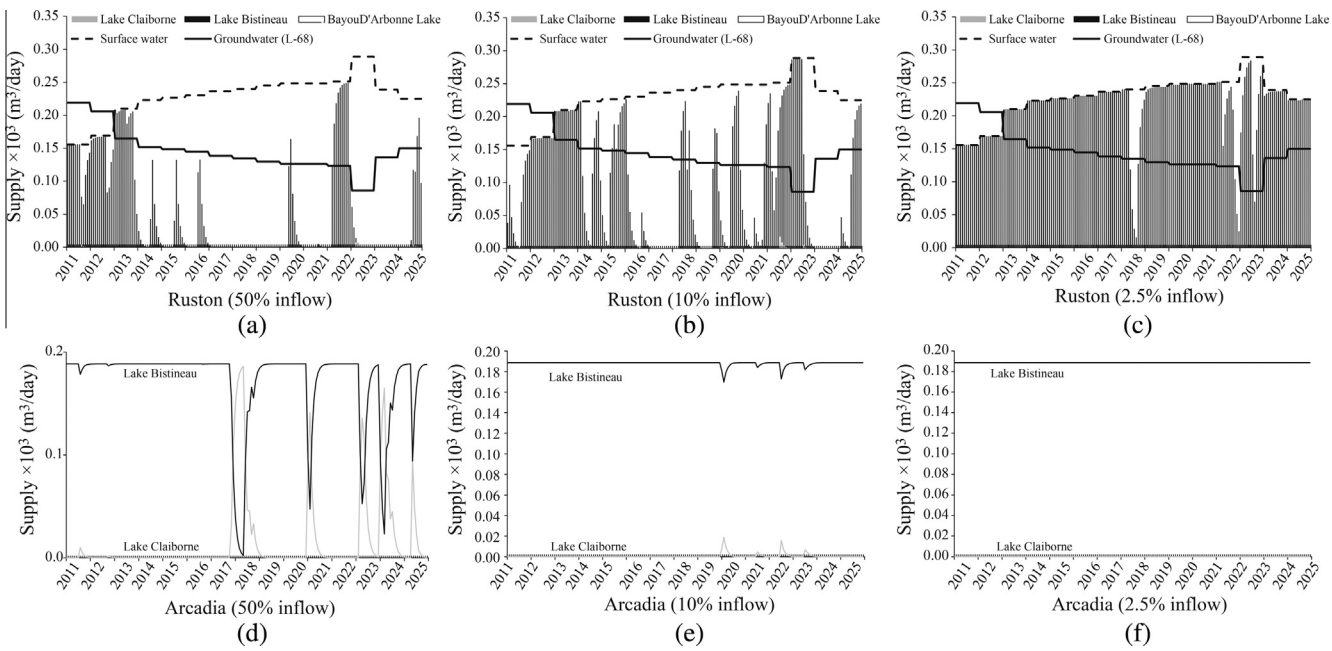

Fig. 13. Optimized surface water and groundwater supplies under 2.5%, 10%, and 50% low reservoir inflow projections for Ruston and Arcadia.

significantly lower than the 68,137 m^3/day (18 MGD) reduction from the Sparta aquifer recommended by Meyer et al. (2002).

3.6. Optimized surface water allocations

The optimized annual groundwater and monthly surface water allocations for Monroe and Farmerville are shown in Fig. 12. Monroe would be a significant user of Bayou D'Arbonne Lake, which would use an average of 132,489 m^3/day (35 MGD) during 2011–2025. About 18% of water demand for Farmerville would come from Bayou D'Arbonne Lake after 2012. Homer would be constantly supplied by Lake Claiborne. The conjunctive-use model suggests that Minden would be constantly supplied by Lake Bistineau, although it might receive surface water from Lake Claiborne. The majority of surface water to Ruston would be shifted from Bayou D'Arbonne Lake to Lake Bistineau, as shown in Fig. 13a–c as inflows decreases. The majority of surface water for Arcadia would come from Lake Bistineau, as shown in Fig. 13d and f. As inflows decrease, Arcadia would receive less water from Lake Claiborne. For the 2.5% low inflow case, Lake Bistineau would supply 100% of the water to Arcadia.

The result indicates that Lake Bistineau would be a reliable surface water supply source to Ruston and Arcadia. At the 2.5% low inflow, Bayou D'Arbonne Lake would not be able to contribute major surface water to Ruston because it would need to fulfill the water demand for Monroe and Farmerville first. Similarly, Lake Claiborne would not be able to supply surface water to Arcadia, as it would need to fulfill the water demand for Homer first.

4. Conclusion

The MILFP provides a simple, computationally efficient approach to optimize conflicting objectives. For a conjunctive use, the successive MILFP is suitable for optimizing groundwater and surface water uses by integrating a groundwater model and a multi-reservoir water supply network model through the response matrix approach. This study expands the Charnes-Cooper transformation technique to include integer variables so that the optimal solution for the successive MILFP problem can be efficiently obtained by solving a successive MILP problem. The proposed conjunctive-use model for the case study successfully demonstrates this technique.

Future inflow estimates to the reservoirs rely on future runoff projections, which present the key uncertainty to the conjunctive management. Through the BMA analysis on an ensemble of 11 sets of downscaled hydroclimate projections, this study found that the near future runoff (2011–2049) for northern Louisiana would be likely to decrease in winter, but it would be likely to increase in spring, summer and fall. Overall, northern Louisiana would likely be in a wetter condition in the near future.

Due to the projected wetter condition, the conjunctive-use modeling result indicates that water demands in northern Louisiana for the future period (2011–2025) would be satisfied even with a 2.5% low inflow projection and a rising groundwater level in the Sparta aquifer. Future surface water would counterbalance the groundwater pumping reduction. It was found that a significant reduction in groundwater withdrawal in Ouachita would elevate the overall groundwater level for northern Louisiana. The conjunctive-use model showed that the target groundwater levels would be met by 2025 by reducing annual groundwater pumpage by 13,703 m^3/day (3.62 MGD).

Through the conjunctive-use model, it was determined that Lake Bistineau would be a reliable future surface water source to Ruston and Arcadia given the proposed network configuration. For the 2.5% low inflow projection, Bayou D'Arbonne Lake would not be able to provide a large amount of surface water to Ruston, as it would have to first satisfy Farmerville and Monroe demands. Similarly, Lake Claiborne would not be able to provide a noticeable amount of surface to Arcadia at a very low projected inflow because it would have to satisfy Homer demands first.

Acknowledgements

This work was supported in part by the Louisiana Board of Regents under award number LEQSF(2012-15)-RD-A-03 and by the U.S. Geological Survey under Grant/Cooperative Agreement No. G11AP20082 (through LWRRI). The authors acknowledge Brian Clark of USGS for providing the Sparta groundwater model, Pierre Sargent of USGS for providing water use data for northern Louisiana, and the Louisiana Sparta Ground Water Commission for providing technical reports. The LSU Center for Computation & Technology (CCT) and the High Performance Computing (HPC) are acknowledged for providing computing resources and technical assistance. This paper was coauthored by employees of the Oak Ridge National Laboratory, managed by UT Battelle, LLC, under contract DE-AC05-00OR22725 with the U.S. Department of Energy. Accordingly, the publisher, by accepting the article for publication, acknowledges that the United States government retains a nonexclusive, paid-up, irrevocable, worldwide license to publish or reproduce the published form of this manuscript, or allow others to do so, for United States government purposes.

Appendix A. Conditional head constraint linearization

This study introduces an equivalent set of inequality constraints (A1)–(A3) to represent the conditional head constraint (9) as follows:

$$\mathbf{h}_{t+1} - \mathbf{h}_t - \mathrm{diag}(\boldsymbol{\Delta}_1 + \boldsymbol{\Delta}_2)\mathbf{u}_t \geqslant -\boldsymbol{\Delta}_2, \tag{A1}$$

$$\mathbf{h}_t + \mathrm{diag}(\mathbf{h}^{\mathrm{target}} - \mathbf{L}_h)\mathbf{u}_t \geqslant \mathbf{h}^{\mathrm{target}}, \text{ and} \tag{A2}$$

$$\mathbf{h}_t + \mathrm{diag}(\mathbf{U}_h - \mathbf{h}^{\mathrm{target}})\mathbf{u}_t < \mathbf{U}_h, \tag{A3}$$

where $\mathbf{u}_t$ is the vector of binary variables at time t, $\mathbf{L}_h$ is the vector of the lower bound for groundwater head at control locations, and $\mathbf{U}_h$ is the vector of the upper bound for groundwater head at control locations. diag(·) makes a vector become a diagonal matrix. $\mathbf{u}_t = \mathbf{0}$ indicates $\mathbf{h}_t \geqslant \mathbf{h}^{\mathrm{target}}$ and $\mathbf{u}_t = \mathbf{1}$ indicates $\mathbf{h}_t < \mathbf{h}^{\mathrm{target}}$.

Using the first-order Taylor series expansion (Peralta et al., 1991; Theodossiou, 2004), groundwater head, $\mathbf{h}_t$, is linearized with respect to pumping rate $\mathbf{Q}_n$ as follows:

$$\mathbf{h}_t^{k+1} \approx \mathbf{h}_t^k + \mathbf{J}_t^k\left(\mathbf{Q}_n^{k+1} - \mathbf{Q}_n^k\right), \tag{A4}$$

where $\mathbf{J}_t^k = \partial\mathbf{h}_t/\partial\mathbf{Q}|_{\mathbf{Q}=\mathbf{Q}_n^k}$ is the Jacobian matrix, $\mathbf{Q}_n^k$ is the vector of pumping rate at the kth iteration, and $\mathbf{h}_t^k = \mathbf{h}_t\left(\mathbf{Q}_n^k\right)$. Substituting Eq. (A4) into constraints (A1)–(A3), linear constraints at the kth iteration are obtained:

$$\left(\mathbf{J}_{t+1}^k - \mathbf{J}_t^k\right)\mathbf{Q}_n^{k+1} - \mathrm{diag}(\boldsymbol{\Delta}_1 + \boldsymbol{\Delta}_2)\mathbf{u}_t \geqslant -\boldsymbol{\Delta}_2 - \left(\mathbf{h}_{t+1}^k - \mathbf{h}_t^k\right) + \left(\mathbf{J}_{t+1}^k - \mathbf{J}_t^k\right)\mathbf{Q}_n^k, \tag{A5}$$

$$\mathbf{J}_t^k\mathbf{Q}_n^{k+1} + \mathrm{diag}(\mathbf{h}^{\mathrm{target}} - \mathbf{L}_h)\mathbf{u}_t \geqslant \mathbf{h}^{\mathrm{target}} - \mathbf{h}_t^k + \mathbf{J}_t^k\mathbf{Q}_n^k, \text{ and} \tag{A6}$$

$$\mathbf{J}_t^k\mathbf{Q}_n^{k+1} + \mathrm{diag}(\mathbf{U}_h - \mathbf{h}^{\mathrm{target}})\mathbf{u}_t \leqslant \mathbf{U}_h - \mathbf{h}_t^k + \mathbf{J}_t^k\mathbf{Q}_n^k, \tag{A7}$$

where $\mathbf{J}_{t+1}^k$, $\mathbf{J}_t^k$, and $\mathbf{Q}_n^k$ are known values from the previous iteration, k, and $\mathbf{Q}_n^{k+1}$ are the decision variables (unknown) to be determined at the current iteration, $k + 1$. A procedure is needed to successively improve the solution until a stopping criterion is met.

Appendix B. Transformation of MILFP to MILP

Following the details provided in Appendix A, the fractional programming problem can be rewritten into a successive mixed-integer linear fractional programming problem (MILFP) as follows:

$$\text{Maximize}\frac{\sum_n \mathbf{1}^T\mathbf{Q}_n^{k+1}}{\sum_t \mathbf{1}^T(\mathbf{S}_{\max} - \mathbf{S}_t) + \beta}, \tag{B1}$$

subject to

$$\left(\mathbf{J}_{t+1}^k - \mathbf{J}_t^k\right)\mathbf{Q}_n^{k+1} - \mathrm{diag}(\boldsymbol{\Delta}_1 + \boldsymbol{\Delta}_2)\mathbf{u}_t \geqslant -\boldsymbol{\Delta}_2 - \left(\mathbf{h}_{t+1}^k - \mathbf{h}_t^k\right) + \left(\mathbf{J}_{t+1}^k - \mathbf{J}_t^k\right)\mathbf{Q}_n^k, \tag{B2}$$

$$\mathbf{J}_t^k\mathbf{Q}_n^{k+1} + \mathrm{diag}(\mathbf{h}^{\mathrm{target}} - \mathbf{L}_h)\mathbf{u}_t \geqslant \mathbf{h}^{\mathrm{target}} - \mathbf{h}_t^k + \mathbf{J}_t^k\mathbf{Q}_n^k, \tag{B3}$$

$$\mathbf{J}_t^k\mathbf{Q}_n^{k+1} + \mathrm{diag}(\mathbf{U}_h - \mathbf{h}^{\mathrm{target}})\mathbf{u}_t \leqslant \mathbf{U}_h - \mathbf{h}_t^k + \mathbf{J}_t^k\mathbf{Q}_n^k, \tag{B4}$$

$$\mathbf{S}_{t+1} = \mathbf{S}_t + \mathbf{I}_t + \sum_{j\in\mathrm{IN}}\mathbf{Sp}_t^{(j)} - \mathbf{R}_t - \mathbf{Sp}_t - \mathbf{E}_t, \text{ and} \tag{B5}$$

$$\sum_{i\in\mathrm{OUT}}\mathbf{x}_t^{(i)} - \sum_{j\in\mathrm{IN}}\mathbf{x}_t^{(j)} = \mathbf{b}_t. \tag{B6}$$

Following Charnes and Cooper (1962), a new variable is introduced:

$$\psi = \frac{1}{\sum_t \mathbf{1}^T(\mathbf{S}_{\max} - \mathbf{S}_t) + \beta}, \tag{B7}$$

where $\psi \geqslant 0$. Then, all variables are multiplied by ψ, resulting in new variables, as follows:

$$\bar{\mathbf{X}} = [\overline{\mathbf{Q}}_n, \overline{\mathbf{S}}_t, \overline{\mathbf{R}}_t, \overline{\mathbf{Sp}}_t, \bar{\mathbf{x}}_t]^T = [\mathbf{Q}_n\psi, \mathbf{S}_t\psi, \mathbf{R}_t\psi, \mathbf{Sp}_t\psi, \mathbf{x}_t\psi]^T, \text{ and} \tag{B8}$$

$$\bar{\mathbf{u}}_t = \mathbf{u}_t\psi = \{0, \psi\}. \tag{B9}$$

By multiplying the MILFP constraints with ψ and substituting them with new variables, the original MIFLP problem is transformed to the following mixed-integer nonlinear programming problem (MINLP):

$$\text{Maximize} \sum_n \mathbf{1}^T \overline{\mathbf{Q}}_{\mathbf{n}}^{\mathbf{k+1}}, \tag{B10}$$

subject to

$$\left(\mathbf{J}_{t+1}^k - \mathbf{J}_t^k\right)\overline{\mathbf{Q}}_n^{k+1} - \text{diag}(\Delta_1 + \Delta_2)\bar{\mathbf{u}}_t + \left[\Delta_2 + \left(\mathbf{h}_{t+1}^k - \mathbf{h}_t^k\right) - \left(\mathbf{J}_{t+1}^k - \mathbf{J}_t^k\right)\mathbf{Q}_n^k\right]\psi \geqslant 0, \tag{B11}$$

$$\mathbf{J}_t^k\overline{\mathbf{Q}}_n^{k+1} + \text{diag}(\mathbf{h}^{\text{target}} - \mathbf{L}_h)\bar{\mathbf{u}}_t - \left[\mathbf{h}^{\text{target}} - \mathbf{h}_t^k + \mathbf{J}_t^k\mathbf{Q}_n^k\right]\psi \geqslant 0, \tag{B12}$$

$$\mathbf{J}_t^k\overline{\mathbf{Q}}_n^{k+1} + \text{diag}(\mathbf{U}_h - \mathbf{h}^{\text{target}})\bar{\mathbf{u}}_t - \left[\mathbf{U}_h - \mathbf{h}_t^k + \mathbf{J}_t^k\mathbf{Q}_n^k\right]\psi \leqslant 0, \tag{B13}$$

$$\bar{\mathbf{S}}_{t+1} = \bar{\mathbf{S}}_t + \mathbf{I}_t\psi + \sum_{j\in\text{IN}}\overline{\mathbf{Sp}}_t^{(j)} - \bar{\mathbf{R}}_t - \overline{\mathbf{Sp}}_t - \mathbf{E}_t\psi, \text{ and} \tag{B14}$$

$$\sum_{i\in\text{OUT}}\bar{\mathbf{x}}_t^{(i)} - \sum_{j\in\text{IN}}\bar{\mathbf{x}}_t^{(j)} = \mathbf{b}_t\psi. \tag{B15}$$

To ensure that Eq. (B7) is satisfied in the new formation, another constraint is imposed:

$$\sum_t \mathbf{1}^T(\mathbf{S}_{\max}\psi - \bar{\mathbf{S}}_{\mathbf{t}}) + \beta\psi = 1. \tag{B16}$$

The ψ multiplication also applies to the bound constraints of the variables in Eq. (B8):

$$\bar{\mathbf{X}} - \mathbf{X}_{\min}\psi \geqslant 0 \text{ and } \bar{\mathbf{X}} - \mathbf{X}_{\max}\psi \leqslant 0. \tag{B17}$$

The discontinuous variables product term $\bar{\mathbf{u}}_t$ in the constraints (B11)–(B13) imposes additional nonlinearity. To address with the discontinuous variables, the following constraints are added:

$$\bar{\mathbf{u}}_t - U\mathbf{u}_t \leqslant \mathbf{0}, \tag{B18}$$

$$L\mathbf{u}_t - \bar{\mathbf{u}}_t \leqslant \mathbf{0}, \tag{B19}$$

$$\psi - \bar{\mathbf{u}}_t + U\mathbf{u}_t \leqslant U, \text{ and} \tag{B20}$$

$$\bar{\mathbf{u}}_t - L\mathbf{u}_t - \psi \leqslant -L, \tag{B21}$$

so that $\bar{\mathbf{u}}_t$ can be treated as continuous variables. L is a negative value, and U is an upper bound of ψ. By adding the constraints (B18)–(B21), the successive MINLP problem becomes a successive mixed-integer linear programming (MILP) problem.

Appendix C. Supplementary material

Supplementary data associated with this article can be found, in the online version, at http://dx.doi.org/10.1016/j.jhydrol.2016.06.021. These data include Google maps of the most important areas described in this article.

References

Ahmed, K.F., Wang, G., Silander, J., Wilson, A.M., Allen, J.M., Horton, R., Anyah, R., 2013. Statistical downscaling and bias correction of climate model outputs for climate change impact assessment in the US northeast. Global Planet. Change 100, 320–332.

Ajami, N.K., Duan, Q., Gao, X., Sorooshian, S., 2006. Multimodel combination techniques for analysis of hydrological simulations: application to distributed model intercomparison project results. J. Hydrometeorol. 7 (4), 755–768. http://dx.doi.org/10.1175/JHM519.1.

Ashfaq, M.L., Bowling, C., Cherkauer, K., Pal, J.S., Diffenbaugh, N.S., 2010. Influence of climate model biases and daily-scale temperature and precipitation events on hydrological impacts assessment: a case study of the United States. J. Geophys. Res.: Atmos. 115 (D14). http://dx.doi.org/10.1029/2009JD012965.

Ashfaq, M., Ghosh, S., Kao, S.-C.C., Bowling, L.C., Mote, P., Touma, D., Rauscher, S.A., Diffenbaugh, N.S., 2013. Near-term acceleration of hydroclimatic change in the western US. J. Geophys. Res.: Atmos. 118 (19), 10676–10693.

Bastola, S., Murphy, C., Sweeney, J., 2011. The role of hydrological modelling uncertainties in climate change impact assessments of Irish river catchments. Adv. Water Resour. 34 (5), 562–576. http://dx.doi.org/10.1016/j.advwatres.2011.01.008.

Bazargan-Lari, M., Kerachian, R., Mansoori, A., 2009. A conflict-resolution model for the conjunctive use of surface and groundwater resources that considers water-quality issues: a case study. Environ. Manage. 43 (3), 470–482. http://dx.doi.org/10.1007/s00267-008-9191-6.

Bhattacharjya, R.K., Datta, B., 2005. Optimal management of coastal aquifers using linked simulation optimization approach. Water Resour. Manage. 19 (3), 295–320. http://dx.doi.org/10.1007/s11269-005-3180-9.

Bosshard, T., Carambia, M., Goergen, K., Kotlarski, S., Krahe, P., Zappa, M., Schär, C., 2013. Quantifying uncertainty sources in an ensemble of hydrological climate-impact projections. Water Resour. Res. 49 (3), 1523–1536. http://dx.doi.org/10.1029/2011WR011533.

Brakebill, J.W., Wolock, D.M., Terziotti, S.E., 2011. Digital hydrologic networks supporting applications related to spatially referenced regression modeling. J. Am. Water Resour. Assoc. 47 (5), 916–932. http://dx.doi.org/10.1111/j.1752-1688.2011.00578.x.

Brekke, L., Wood, A., Pruitt, T., 2013. Downscaled CMIP3 and CMIP5 Hydrology Projections: Release of Hydrology Projections, Comparison with Preceding Information, and Summary of User Needs. U.S. Department of the Interior, Bureau of Reclamation, Technical Services Center, Denver, CO.

Buser, C.M., Künsch, H.R., Lüthi, D., Wild, M., Schär, C., 2009. Bayesian multi-model projection of climate: bias assumptions and interannual variability. Clim. Dynam. 33 (6), 849–868. http://dx.doi.org/10.1007/s00382-009-0588-6.

Charnes, A., Cooper, W.W., 1962. Programming with linear fractional functionals. Naval Res. Logist. Quart. 9 (3–4), 181–186. http://dx.doi.org/10.1002/nav.3800090303.

Christensen, N.S., Wood, A.W., Voisin, N., Lettenmaier, D.P., Palmer, R.N., 2004. The effects of climate change on the hydrology and water resources of the Colorado River basin. Clim. Change 62 (1–3), 337–363. http://dx.doi.org/10.1023/B:CLIM.0000013684.13621.1f.

Daly, C., Halbleib, M., Smith, J.I., Gibson, W.P., Doggett, M.K., Taylor, G.H., Curtis, J., Pasteris, P.P., 2008. Physiographically sensitive mapping of climatological temperature and precipitation across the conterminous United States. Int. J. Climatol. 28 (15), 2031–2064. http://dx.doi.org/10.1002/joc.1688.

Diffenbaugh, N.S., Ashfaq, M., Scherer, M., 2011. Transient regional climate change: analysis of the summer climate response in a high-resolution, century-scale, ensemble experiment over the continental United States. J. Geophys. Res. 116 (D24). http://dx.doi.org/10.1029/2011JD016458.

Dong, L., Xiong, L., Yu, K., 2013. Uncertainty analysis of multiple hydrologic models using the Bayesian model averaging method. J. Appl. Math. 2013, 1–11. http://dx.doi.org/10.1155/2013/346045.

Draper, D., 1995. Inference and hierarchical modeling in the social sciences. J. Educat. Behav. Stat. 20 (2), 115–147.

Duan, Q., Ajami, N.K., Gao, X., Sorooshian, S., 2007. Multi-model ensemble hydrologic prediction using Bayesian model averaging. Adv. Water Resour. 30 (5), 1371–1386. http://dx.doi.org/10.1016/j.advwatres.2006.11.014.

Fasakhodi, A., Nouri, S., Amini, M., 2010. Water resources sustainability and optimal cropping pattern in farming systems: a multi-objective fractional goal programming approach. Water Resour. Manage. 24 (15), 4639–4657. http://dx.doi.org/10.1007/s11269-010-9683-z.

Gesch, D., Oimoen, M., Greenlee, S., Nelson, C., Steuck, M., Tyler, D., 2002. The national elevation dataset. Photogramm. Eng. Rem. Sens. 68 (1), 5–11.

Giorgi, F., Coppola, E., Solmon, F., Mariotti, L., Sylla, M.B., Bi, X., Elguindi, N., Diro, G.T., Nair1, V., Giuliani, G., Turuncoglu, U.U., Cozzini, S., Güttler, I., O'Brien, T.A., Tawfik, A.B., Shalaby, A., Zakey, A.S., Steiner, A.L., Stordal, F., Sloan, L.C., Turuncoglu, U.U., 2012. RegCM4: model description and preliminary tests over multiple CORDEX domains. Clim. Res. 2 (7), 7–29. http://dx.doi.org/10.3354/cr01018.

Guo, P., Chen, X., Li, M., Li, J., 2014. Fuzzy chance-constrained linear fractional programming approach for optimal water allocation. Stoch. Env. Res. Risk Assess. 28 (6), 1601–1612. http://dx.doi.org/10.1007/s00477-013-0810-2.

Hagemann, S., Chen, C., Clark, D., Folwell, S., Gosling, S.N., Haddeland, I., Hannasaki, N., Heinke, J., Ludwig, F., Voss, F., Wiltshire, A.J., 2013. Climate change impact on available water resources obtained using multiple global climate and hydrology models. Earth Syst. Dynam. 4, 129–144. http://dx.doi.org/10.5194/esd-4-129-2013.

Hoeting, J.A., Madigan, D., Raftery, A.E., Volinsky, C.T., 1999. Bayesian model averaging: a tutorial. Stat. Sci., 382–401

IBM, 2009. IBM ILOG CPLEX Computer Program, Version 12.1, Armonk, NY, International Business Machines Corporation.

Katsifarakis, K.L., Petala, Z., 2006. Combining genetic algorithms and boundary elements to optimize coastal aquifers' management. J. Hydrol. 327 (1–2), 200–207. http://dx.doi.org/10.1016/j.jhydrol.2005.11.016.

LaDNR, 2015. Areas of Ground Water Concerns. Office of Conservation, Louisiana Department of Natural Resources. Available on the World Wide Web, at URL. <http://dnr.louisiana.gov/index.cfm?md=pagebuilder&tmp=home&pid=473> (accessed May 7, 2015).

Lara, P., Stancu-Minasian, I., 1999. Fractional programming: a tool for the assessment of sustainability. Agric. Syst. 62 (2), 131–141. http://dx.doi.org/10.1016/S0308-521X(99)00062-1.

Liang, X., Lettenmaier, D.P., Wood, E.F., Burges, S.J., 1994. A simple hydrologically based model of land surface water and energy fluxes for general circulation models. J. Geophys. Res.: Atmos. 99 (D7), 14415–14428. http://dx.doi.org/10.1029/94JD00483.

Liang, X., Wood, E.F., Lettenmaier, D.P., 1996. Surface soil moisture parameterization of the VIC-2L model: evaluation and modification. Global Planet. Change 13 (1), 195–206. http://dx.doi.org/10.1016/0921-8181(95)00046-1.

Liang, Z., Wang, D., Guo, Y., Zhang, Y., Dai, R., 2013. Application of bayesian model averaging approach to multimodel ensemble hydrologic forecasting. J. Hydrol. Eng. 18 (11), 1426–1436. http://dx.doi.org/10.1061/(ASCE)HE.1943-5584.0000493.

Lohmann, D., Raschke, E., Nijssen, B., Lettenmaier, D.P., 1998. Regional scale hydrology, part 1: formulation of the VIC-2L model coupled to a routing model. Hydrol. Sci. J. 43, 131–141. http://dx.doi.org/10.1080/02626669809492107.

Mahoney, K., Alexander, M.A., Thompson, G., Barsugli, J.J., Scott, J.D., 2012. Changes in hail and flood risk in high-resolution simulations over Colorado's mountains. Nat. Clim. Change 2 (2), 125–131. http://dx.doi.org/10.1038/nclimate1344.

Mantoglou, A., 2003. Pumping management of coastal aquifers using analytical models of saltwater intrusion. Water Resour. Res. 39 (12), 1335. http://dx.doi.org/10.1029/2002WR001891.

McKee, P.W., Clark, B.R., 2003. Development and Calibration of a Groundwater Flow Model for the Sparta Aquifer of Southeastern Arkansas and North-Central Louisiana and Simulated Response to Withdrawals, 1998–2027. USGS Water-Resources Investigations Report 03-4132.

Meyer, Meyer, LeCroix, Hixson Inc., Lazenby and Associates, Louisiana Tech University, URS Corporation, Charles W. Smoot and Frye-Magee, 2002. Sparta Groundwater Study: A Study Commissioned By the Sparta Groundwater Conservation District Commission, Louisiana.

Milly, P.C., Dunne, K.A., Vecchia, A.V., 2005. Global pattern of trends in streamflow and water availability in a changing climate. Nature 438 (7066), 347–350. http://dx.doi.org/10.1038/nature04312.

Min, S.K., Simonis, D., Hense, A., 2007. Probabilistic climate change predictions applying Bayesian model averaging. Philos. Trans. Roy. Soc. Lond. A: Math., Phys. Eng. Sci. 365 (1857), 2103–2116. http://dx.doi.org/10.1098/rsta.2007.2070.

Mohammad Rezapour Tabari, M., Yazdi, A., 2014. Conjunctive use of surface and groundwater with inter-basin transfer approach: case study Piranshahr. Water Resour. Manage. 28 (8), 1887–1906. http://dx.doi.org/10.1007/s11269-014-0578-2, Springer.

Mulholland, P.J., Best, G.R., Coutant, C.C., Hornberger, G.M., Meyer, J.L., Robinson, P.J., Stenberg, J.R., Turner, R.E., Vera-Herrera, F., Wetzel, R.G., 1997. Effects of climate change on freshwater ecosystems of the south-eastern United States and the Gulf Coast of Mexico. Hydrol. Process. 11 (8), 949–970. http://dx.doi.org/10.1002/(SICI)1099-1085(19970630)11:8<949::AID-HYP513>3.0.CO;2-G.

Najafi, M.R., Moradkhani, H., Jung, I.W., 2011. Assessing the uncertainties of hydrologic model selection in climate change impact studies. Hydrol. Process. 25 (18), 2814–2826. http://dx.doi.org/10.1002/hyp.8043.

Oubeidillah, A.A., Kao, S.C., Ashfaq, M., Naz, B.S., Tootle, G., 2014. A large-scale, high-resolution hydrological model parameter data set for climate change impact assessment for the conterminous US. Hydrol. Earth Syst. Sci. 18 (1), 67–84. http://dx.doi.org/10.5194/hess-18-67-2014.

Peralta, R.C., Azarmnia, H., Takahashi, S., 1991. Embedding and response matrix techniques for maximizing steady-state ground-water extraction: computational comparison. Ground Water 29 (3), 357–364. http://dx.doi.org/10.1111/j.1745-6584.1991.tb00526.x.

Peters, G.P., Andrew, R.M., Boden, T., Canadell, J.G., Ciais, P., Le Quéré, C., Marland, G., Raupach, M.R., Wilson, C., 2013. The challenge to keep global warming below 2 °C. Nat. Clim. Change 3 (1), 4–6. http://dx.doi.org/10.1038/nclimate1783.

Raftery, A.E., Zheng, Y., 2003. Long-run performance of Bayesian model averaging. J. Am. Stat. Assoc. 98 (464), 931–938. http://dx.doi.org/10.1198/016214503000000891.

Ramesh, H., Mahesha, A., 2008. Simulation of varada aquifer system for sustainable groundwater development. J. Irrigat. Drain. Eng. 134 (3), 387–399. http://dx.doi.org/10.1061/(ASCE)0733-9437(2008) 134:3(387).

Ren, C.F., Guo, P., Li, M., Gu, J.J., 2013. Optimization of industrial structure considering the uncertainty of water resources. Water Resour. Manage. 27 (11), 3885–3898. http://dx.doi.org/10.1007/s11269-013-0385-1.

Rojas, R., Feyen, L., Dosio, A., Bavera, D., 2011. Improving pan-European hydrological simulation of extremeeventsthrough statistical bias correction of RCM-driven climatesimulations. Hydrol. Earth Syst. Sci. 15 (8), 2599–2620. http://dx.doi.org/10.5194/hess-15-2599-2011.

Sargent, B.P., 2012. Water Use in Louisiana, 2010, Louisiana Department of Transportation and Development, Water Resources Special Report No. 17 (Revised), 135p.

Schaible, S., 1981. Fractional programming: applications and algorithms. Eur. J. Oper. Res. 7 (2), 111–120. http://dx.doi.org/10.1016/0377-2217(81)90272-1.

Schwarz, G., 1978. Estimating the dimension of a model. Ann. Stat. 6 (2), 461–464.

Seager, R., Ting, M., Li, C., Naik, N., Cook, B., Nakamura, J., Liu, H., 2013. Projections of declining surface-water availability for the southwestern United States. Nat. Clim. Change 3 (5), 482–486. http://dx.doi.org/10.1038/nclimate1787.

Singh, A., 2012. An overview of the optimization modelling applications. J. Hydrol. 466, 167–182. http://dx.doi.org/10.1016/j.jhydrol.2012.08.004.

Singh, A., 2014. Conjunctive use of water resources for sustainable irrigated agriculture. J. Hydrol. 519 (B), 1688–1697. http://dx.doi.org/10.1016/j.jhydrol.2014.09.049.

Smith, R.L., Tebaldi, C., Nychka, D., Mearns, L.O., 2009. Bayesian modeling of uncertainty in ensembles of climate models. J. Am. Stat. Assoc. 104 (485), 97–116. http://dx.doi.org/10.1198/jasa.2009.0007.

Stocker, T., Dahe, Q., Plattner, G.-K., Tignor, M., Midgley, P., 2010. IPCC Expert Meeting on Assessing and Combining Multi Model Climate Projections. National Center for Atmospheric Research, Boulder, Colorado, USA, pp. 25–27.

Tamer Ayvaz, M., Karahan, H., 2008. A simulation/optimization model for the identification of unknown groundwater well locations and pumping rates. J. Hydrol. 357 (1–2), 76–92. http://dx.doi.org/10.1016/j.jhydrol.2008.05.003.

Tebaldi, C., Smith, R.L., Nychka, D., Mearns, L.O., 2005. Quantifying uncertainty in projections of regional climate change: a Bayesian approach to the analysis of multimodel ensembles. J. Clim. 18 (10), 1524–1540. http://dx.doi.org/10.1175/JCLI3363.1.

Theodossiou, N.P., 2004. Application of non-linear simulation and optimisation models in groundwater aquifer management. Water Resour. Manage. 18 (2), 125–141. http://dx.doi.org/10.1023/B:WARM.0000024723.17916.64.

Thornton, P.E., Running, S.W., White, M.A., 1997. Generating surfaces of daily meteorological variables over large regions of complex terrain. J. Hydrol. 190 (3), 214–251. http://dx.doi.org/10.1016/S0022-1694(96)03128-9.

Tsai, F.T.-C., Li, X., 2008. Inverse groundwater modeling for hydraulic conductivity estimation using Bayesian model averaging and variance window. Water Resour. Res. 44 (9). http://dx.doi.org/10.1029/2007wr006576.

USACE, 2015. U.S. Army Corps of Engineers, CorpsMap National Inventory of Dams, Reservoir data available on the World Wide Web, at URL. <http://nid.usace.army.mil> (accessed March 2, 2016).

USEPA and USGS, 2010. NHDPlus User Guide, U.S. Environmental Protection Agency and U.S. Geological Survey, Available At: <ftp://ftp.horizon-systems.com/NHDPlus/NHDPlusV1/documentation/NHDPLUSV1_UserGuide.pdf,> (accessed March 2016).

Vetter, T., Huang, S., Aich, V., Yang, T., Wang, X., Krysanova, V., Hattermann, F., 2015. Multi-model climate impact assessment and intercomparison for three large-scale river basins on three continents. Earth Syst. Dynam. 6 (1), 17–43. http://dx.doi.org/10.5194/esd-6-17-2015.

Vogel, R.M., Stedinger, J.R., 1987. Generalized storage-reliability-yield relationships. J. Hydrol. 89, 303–327. http://dx.doi.org/10.1016/0022-1694(87)90184-3.

Vogel, R.M., Lane, M., Ravindiran, R.S., Kirshen, P., 1999. Storage reservoir behavior in the United States. J. Water Resour. Plan. Manage. 125 (5), 245–254. http://dx.doi.org/10.1061/(ASCE)0733-9496.

Vrugt, J.A., Robinson, B.A., 2007. Treatment of uncertainty using ensemble methods: comparison of sequential data assimilation and Bayesian model averaging. Water Resour. Res. 43 (1). http://dx.doi.org/10.1029/2005WR004838.

Weiland, F.S., Van Beek, L.P.H., Weerts, A.H., Bierkens, M.F.P., 2012. Extracting information from an ensemble of GCMs to reliably assess future global runoff change. J. Hydrol. 412, 66–75. http://dx.doi.org/10.1016/j.jhydrol.2011.03.047.

Zhang, X., Srinivasan, R., Bosch, D., 2009. Calibration and uncertainty analysis of the SWAT model using genetic algorithms and Bayesian model averaging. J. Hydrol. 374 (3–4), 307–317. http://dx.doi.org/10.1016/j.jhydrol.2009.06.023.

Zhu, H., Huang, G.H., 2011. SLFP: a stochastic linear fractional programming approach for sustainable waste management. Waste Manage. 31 (12), 2612–2619. http://dx.doi.org/10.1016/j.wasman.2011.08.009.